

DeepQuantum: A PyTorch-based Software Platform for Quantum Machine Learning and Photonic Quantum Computing

Jun-Jie He^{¶,1,*} Ke-Ming Hu,^{1,*} Yu-Ze Zhu,^{1,*} Guan-Ju Yan,^{2,*} Shu-Yi Liang,^{2,*} Xiang Zhao,¹ Ding Wang,¹ Fei-Xiang Guo,^{2,3} Ze-Feng Lan,^{2,3} Xiao-Wen Shang,^{2,3} Zi-Ming Yin,² Xin-Yang Jiang,² Lin Yang,^{1,†} Hao Tang,^{2,3,‡} and Xian-Min Jin^{1,2,3,4,§}

¹*TuringQ Co., Ltd., Shanghai 200240, China*

²*Center for Integrated Quantum Information Technologies (IQIT),*

*School of Physics and Astronomy and State Key Laboratory of Photonics and Communications,
Shanghai Jiao Tong University, Shanghai 200240, China*

³*Hefei National Laboratory, Hefei 230088, China*

⁴*Chip Hub for Integrated Photonics Xplore (CHIPX),
Shanghai Jiao Tong University, Wuxi 214000, China*

We introduce DeepQuantum, an open-source, PyTorch-based software platform for quantum machine learning and photonic quantum computing. This AI-enhanced framework enables efficient design and execution of hybrid quantum-classical models and variational quantum algorithms on both CPUs and GPUs. For photonic quantum computing, DeepQuantum implements Fock, Gaussian, and Bosonic backends, catering to different simulation needs. Notably, it is the first framework to realize closed-loop integration of three paradigms of quantum computing, namely quantum circuits, photonic quantum circuits, and measurement-based quantum computing, thereby enabling robust support for both specialized and universal photonic quantum algorithm design. Furthermore, DeepQuantum supports large-scale simulations based on tensor network techniques and a distributed parallel computing architecture. We demonstrate these capabilities through comprehensive benchmarks and illustrative examples. With its unique features, DeepQuantum is intended to be a powerful platform for both AI for Quantum and Quantum for AI.

CONTENTS

I. Introduction	2	2. Unitary transformation with Clements structure	14
II. DeepQuantum Overview	3	3. Gaussian Boson sampling	15
III. Benchmarks	3	4. Preparation of EPR state with TDM	16
A. Gradient and Hessian	4	5. Preparation of two-dimensional cluster state with TDM	16
B. Hafnian, Torontonian and permanent	5	6. Generation of Non-Gaussian GKP state	17
C. Transpilation and forward computation	6	VI. Measurement-Based Quantum Computing	19
IV. Quantum Computing with Qubits	6	A. Background	19
A. Background	6	B. API Overview	19
B. API Overview	6	C. Applications	20
C. Applications	7	VII. Large-scale Simulations	20
1. QResNet	7	A. Tensor Network and Matrix Product State	20
2. QCNN	8	B. Distributed Simulations	22
V. Photonic Quantum Computing	9	C. Applications	23
A. Background	9	1. Simulation of Large Quantum System with MPS	23
B. API Overview	11	2. Distributed Quantum Fourier Transform	24
C. Time-Domain Multiplexing	12	VIII. Conclusion	25
D. Applications	13	References	25
1. CNOT based on dual-rail encoding	13	Acknowledgments	28

[¶] hejunjie@turingq.com

* These authors contributed equally to this work.

[†] yanglin@turingq.com

[‡] htang2015@sjtu.edu.cn

[§] xianmin.jin@sjtu.edu.cn

I. INTRODUCTION

Artificial intelligence (AI) and quantum computing (QC), both concepts conceived in the last century, are today at vastly different stages of maturity. While AI has become a transformative technology driving real-world value across countless domains, QC is in a nascent phase, primarily demonstrating its potential through carefully constructed proofs of quantum advantage. The pursuit of this advantage, where quantum devices perform tasks intractable for the most powerful classical supercomputers, has seen remarkable progress in recent years. Landmark experiments, such as quantum random sampling on superconducting and photonic platforms [1–3], have convincingly demonstrated this capability for specific, contrived problems. However, a critical and pressing challenge for the field is to translate these theoretical demonstrations into practical, real-world applications with tangible value. The transition from demonstrating quantum advantage to harnessing quantum utility is of paramount importance.

In the current noisy intermediate-scale quantum (NISQ) era [4], this translation effort relies heavily on the synergy between quantum processors and classical computers. Hybrid quantum-classical algorithms have emerged as the most promising paradigm [5], where a quantum device acts as a specialized co-processor whose parameters are optimized within a classical post-processing and feed-forward loop. Prominent examples that exemplify this approach include the variational quantum eigensolver (VQE) for quantum chemistry [6], the quantum approximate optimization algorithm (QAOA) for combinatorial optimization [7], and a variety of methods in quantum machine learning (QML), such as the quantum reservoir computing and quantum extreme learning machine [8, 9]. These works demonstrate how quantum circuits can be utilized as powerful models within classical AI frameworks to achieve a “quantum-enhanced” effect [10, 11].

As the community looks beyond the NISQ era, the ultimate goal is the realization of fault-tolerant quantum computing (FTQC), which promises to unlock the full potential of seminal algorithms like Shor’s [12] and Grover’s [13]. The journey from noisy, intermediate-scale devices to robust, large-scale fault-tolerant machines is fraught with immense challenges, particularly in areas including quantum error correction (QEC) and circuit compilation. Increasingly, AI is being recognized as an indispensable tool to overcome these hurdles. For instance, machine learning, especially deep reinforcement learning, has shown significant promise in designing more efficient QEC decoders [14, 15] and optimizing the complex process of compiling high-level quantum algorithms into low-level hardware instructions [16, 17].

As established, AI is crucial for advancing QC, from optimizing NISQ-era utilities to paving the way for FTQC. Conversely, the nascent field of QML provides compelling evidence for the reverse. Early studies suggest

that quantum algorithms could enhance AI by offering faster training, improved model performance, or reduced data requirements for specific tasks [18]. This creates a powerful virtuous cycle: AI accelerates the development of quantum hardware, which in turn promises to revolutionize AI itself. This reciprocal relationship underscores a future where the two fields are deeply intertwined.

Given this profound and growing interdependency, the need for a programming framework that deeply and seamlessly integrates AI and QC is paramount. Several pioneering frameworks have emerged to address this, such as PennyLane [19] and TensorFlow Quantum [20], which successfully treat quantum circuits as differentiable components within classical machine learning pipelines. While these tools have significantly advanced the field of QML, researchers may face practical challenges when attempting to couple quantum circuits with the ever-evolving landscape of state-of-the-art AI models. Furthermore, they predominantly focus on the standard qubit-based circuit model. However, to pave a viable path toward FTQC, it is crucial to consider alternative computational models and hardware platforms. Photonic quantum computing, in particular, stands out as a leading candidate due to its inherent advantages, such as low noise profiles, operational simplicity, and its role as a natural “flying qubit” for networking. This versatility has spurred recent breakthroughs, including the generation of integrated photonic Gottesman-Kitaev-Preskill (GKP) qubits [21] and demonstrations of modular, manufacturable computing platforms [22, 23]. Many of these scalable architectures are designed around the measurement-based quantum computing (MBQC) paradigm [24], which is naturally suited for fault-tolerant computation. Existing specialized frameworks, such as Strawberry Fields [25] and Piquasso [26] for continuous-variable (CV) quantum computation, Perceval [27] for discrete-variable (DV) photonic systems, and Graphix [28] for MBQC simulations, have provided invaluable tools for their respective domains, but a unified platform that bridges these models while maintaining a native AI integration is still lacking.

To address these challenges and bridge the existing gaps, we introduce DeepQuantum, a novel programming framework engineered to foster the deep synergy between AI and QC for the NISQ era and beyond. This paper is organized as follows: Section II introduces the DeepQuantum framework, highlighting its global architecture and key features. Section III validates such advantages through benchmark results. Sections IV, V, and VI respectively focus on quantum computation with qubits, photonic quomodes, and MBQC patterns, covering the background, API overview, and application examples. Section VII demonstrates large-scale quantum simulation through tensor network techniques and distributed methods. In Section VIII, we summarize the whole paper and outline the future outlook.

II. DEEPQUANTUM OVERVIEW

The DeepQuantum platform is designed to bridge AI and QC, providing an integrated environment that supports both AI-enhanced quantum algorithms and quantum-enhanced machine learning. Built with an emphasis on efficiency and usability, it offers a high-performance programming framework and an intuitive interface for constructing quantum circuits, allowing developers to prototype and explore advanced quantum applications rapidly.

Implemented in Python and leveraging the widely adopted deep learning framework PyTorch [29], DeepQuantum is fully open-source¹ and can be easily installed via pip:

```
$ pip install deepquantum
```

The overall architecture of DeepQuantum is illustrated in Fig. 1. As an efficient programming framework tailored for quantum machine learning and photonic quantum computing, it achieves a closed-loop integration of three major paradigms: quantum circuits, photonic quantum circuits, and MBQC. At its core, the framework provides three principal classes for quantum computation: `QubitCircuit`, `QumodeCircuit`, and `Pattern`. The `QubitCircuit` class enables users to easily construct and simulate quantum circuits, facilitating the rapid design and optimization of quantum neural networks. The `QumodeCircuit` class includes Fock, Gaussian, and Bosonic backends, allowing in-depth exploration of photonic quantum circuits. Furthermore, `QumodeCircuit` supports the development of practical applications based on time-domain multiplexing (TDM) and Gaussian Boson sampling (GBS) algorithms [30]. The `Pattern` class, along with the built-in transpiler from `QubitCircuit` to `Pattern`, empowers users to extensively investigate the MBQC paradigm. Theoretically, these three paradigms are closely linked and interconvertible. MBQC has been proven to be equivalent to the quantum circuit model. Photonic quantum circuits are natural for generating cluster states by appropriate algorithms. Specifically, DeepQuantum provides `UnitaryMapper` to help transfer `QubitCircuit` to `QumodeCircuit` based on dual-rail encoding. DeepQuantum also supports noisy simulations with built-in noise channels. To support large-scale simulations, DeepQuantum incorporates a distributed parallel computing architecture and leverages tensor network techniques.

Fig. 1 also showcases the central role of DeepQuantum in the ecosystem and as a bridge between high-level quantum algorithms and low-level hardware execution. Through its built-in modules, DeepQuantum can handle universal quantum computing based on qubits, DV, CV, and graph states (see more details in later sections).

On classical hardware (CPUs and GPUs), it utilizes PyTorch’s intuitive API and extensive machine learning libraries to facilitate efficient development and experimentation with hybrid quantum-classical algorithms such as QML, QAOA, and VQE. For execution on photonic quantum processors, DeepQuantum provides built-in non-gradient optimizers to enable on-chip training of quantum machine learning models. In a word, DeepQuantum is used to design algorithms upwards for the users and map algorithms downwards to the chips.

DeepQuantum is built upon the principles of conciseness, efficiency, flexibility, and versatility. Its key features include:

- **AI-Enhanced Quantum Computing Framework:** Seamlessly integrated with PyTorch, it utilizes technologies such as automatic differentiation, vectorized parallelism, and GPU acceleration for efficiency. It facilitates the easy construction of hybrid quantum-classical models, enabling end-to-end training and inference.
- **User-Friendly API Design:** The API is designed to be simple and intuitive, making it easy to initialize quantum neural networks and providing flexibility in data encoding.
- **Photonic Quantum Computing Simulation:** The Photonic module includes Fock, Gaussian, and Bosonic backends, catering to different simulation needs in photonic quantum computing. It comes with built-in optimizers to support on-chip training of photonic quantum circuits.
- **Large-Scale Quantum Circuit Simulation:** Leveraging tensor network techniques, DeepQuantum enables approximate simulation of circuits with over 100 qubits on a single laptop. Through a distributed parallel architecture and PyTorch’s native communication protocol, it efficiently utilizes multi-node, multi-GPU computational power to boost large-scale quantum simulations. These capabilities allow DeepQuantum to deliver industry-leading performance in both simulation scale and efficiency.
- **Advanced Architecture for Cutting-Edge Algorithm Exploration:** It is the first framework to support algorithm design and mapping for TDM photonic quantum circuits, and the first to realize closed-loop integration of quantum circuits, photonic quantum circuits, and MBQC, enabling robust support for both specialized and universal photonic quantum algorithm design.

III. BENCHMARKS

DeepQuantum is designed with a strong emphasis on simulation efficiency, incorporating optimized data struc-

¹ <https://github.com/TuringQ/deepquantum>

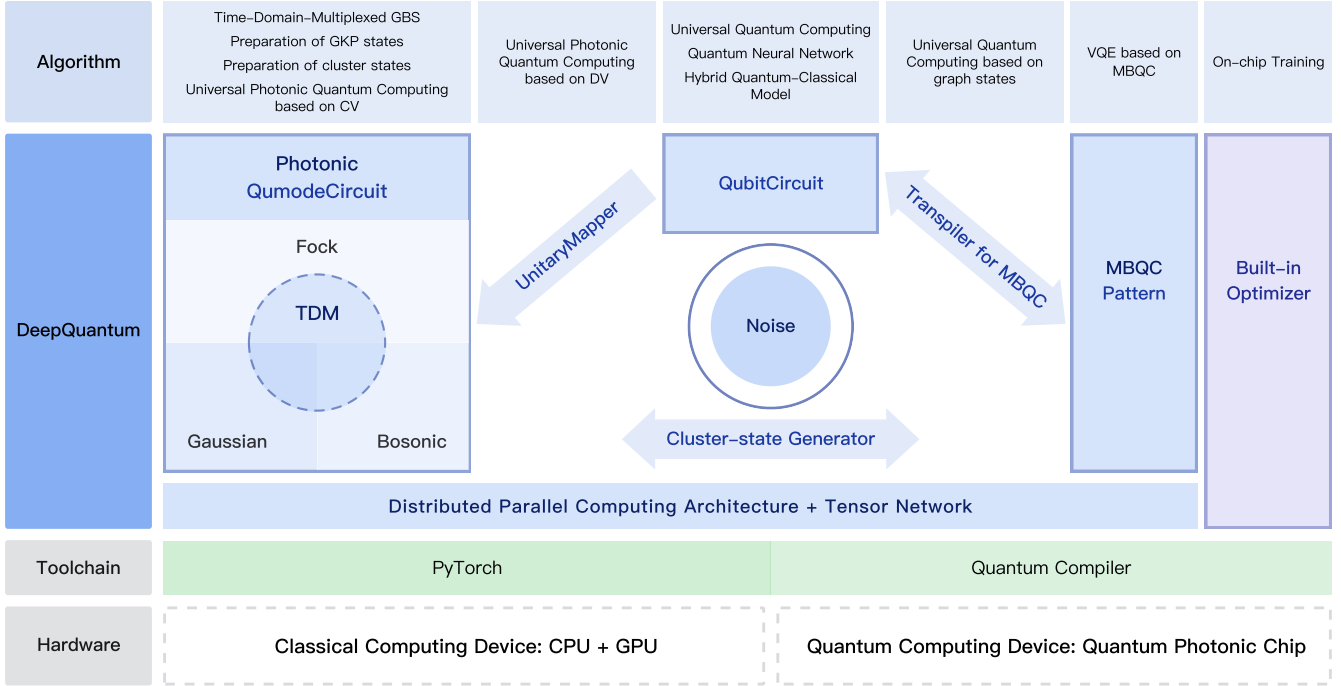


FIG. 1. The architecture of DeepQuantum and its ecosystem, including high-level quantum algorithms, toolchain, and low-level hardware.

tures to enhance runtime performance. In this section, we present benchmarks comparing DeepQuantum against other quantum computing programming frameworks. The evaluation covers core functionalities, including gradient and Hessian calculations for **QubitCircuit**, the computation of Hafnians, Torontonians, and permanents for **QumodeCircuit**, as well as transpilation and forward simulation for **Pattern**. For each benchmark test, it is executed ten times following an initial warm-up iteration. However, the number of repetitions is appropriately decreased if the computational demands of the simulation scale are excessively large.

Table I shows the versions of frameworks used in this test, and Table II shows the main software and hardware environments.

TABLE I. The software version of benchmarking.

Framework	Version
DeepQuantum	4.4.0
PennyLane [19]	0.41.1
MindQuantum [31]	0.10.0
Strawberry Fields [25]	0.23.0
The Walrus [32]	0.22.0
Piquasso [26]	6.0.1
Graphix [28]	0.3.1
PyQPanda3 [33]	0.3.2

TABLE II. The software and hardware environments.

Software/Hardware	Version/Model
PyTorch	2.3.0 + CUDA 12.1
NumPy	1.26.4
CPU	Intel Xeon Gold 6326
GPU	NVIDIA A100

A. Gradient and Hessian

Evaluating the efficiency of gradient and Hessian computation [34] is essential for advancing variational quantum algorithms (VQAs), including VQE and QAOA [35]. Fig. 2(a) presents the benchmark outcomes for gradient computation across different platforms: DeepQuantum, MindQuantum, PennyLane, and PyQPanda3. The benchmarks are performed with varying qubit counts and numbers of layers.

At large scales, DeepQuantum is an order of magnitude more efficient than PennyLane and PyQPanda3. At 18 qubits, DeepQuantum outperforms MindQuantum. Regarding GPU acceleration, starting from 14 qubits, the computational efficiency of DeepQuantum (GPU) surpasses that of CPU-based implementations, ultimately achieving a speedup of more than one order of magnitude. Beyond 18 qubits, DeepQuantum (GPU) emerges as the fastest among all tested platforms.

Fig. 2(b) shows the benchmark results of Hessian computation between DeepQuantum and PennyLane.

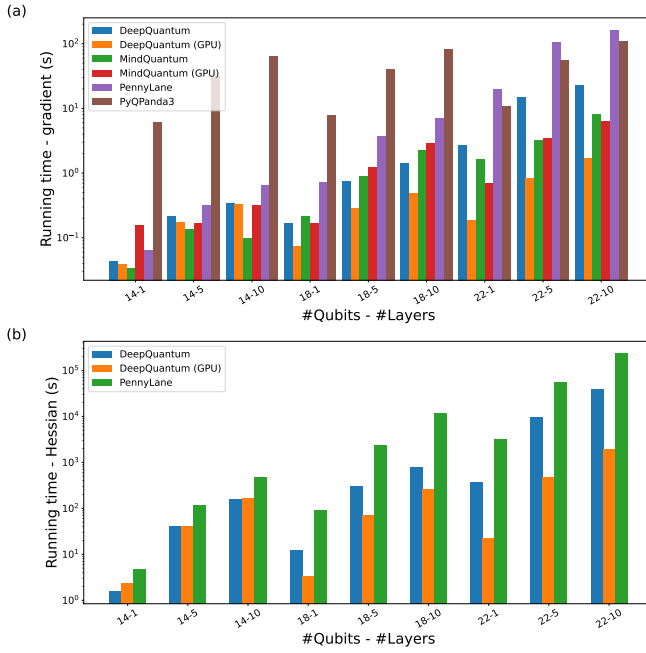


FIG. 2. Benchmark results of gradient (a) and Hessian (b) computation among DeepQuantum, MindQuantum, PennyLane, and PyQPanda.

Benchmark tests are conducted in the same circuit in the gradient benchmark. Benchmark result reveals that DeepQuantum achieves a significantly higher computational speed than PennyLane. This performance advantage becomes particularly pronounced at a larger scale with GPU acceleration.

B. Hafnian, Torontonian and permanent

The evaluation of matrix functions such as the Hafnian [36], Torontonian [37], and permanent [38] plays a fundamental role in photonic quantum simulation. These functions determine the output probability distributions in GBS (Gaussian backend) and DV (Fock backend) models. Although these computations are generally $\#P$ -hard and classically intractable for large-scale problems, their efficient evaluation remains essential for benchmarking, verification, and small-to-medium-scale simulations in hybrid quantum-classical workflows.

DeepQuantum implements a batch-processing scheme for computing Hafnian, Torontonian, and permanent functions. Batch processing enables simultaneous evaluation of multiple quantum circuit instances, significantly improving throughput and resource utilization on GPU and multi-core systems. This approach is particularly advantageous in AI-driven tasks, such as training variational photonic circuits or running large-scale parameter scans, where the ability to process many inputs in parallel can compensate for individual computational overhead.

It should be noted, however, that our current im-

plementation does not include low-level, architecture-specific optimizations for these matrix functions. As a result, in single-instance computations, DeepQuantum may be slower than specialized libraries such as Strawberry Fields or Piquasso, which use highly optimized numerical backends.

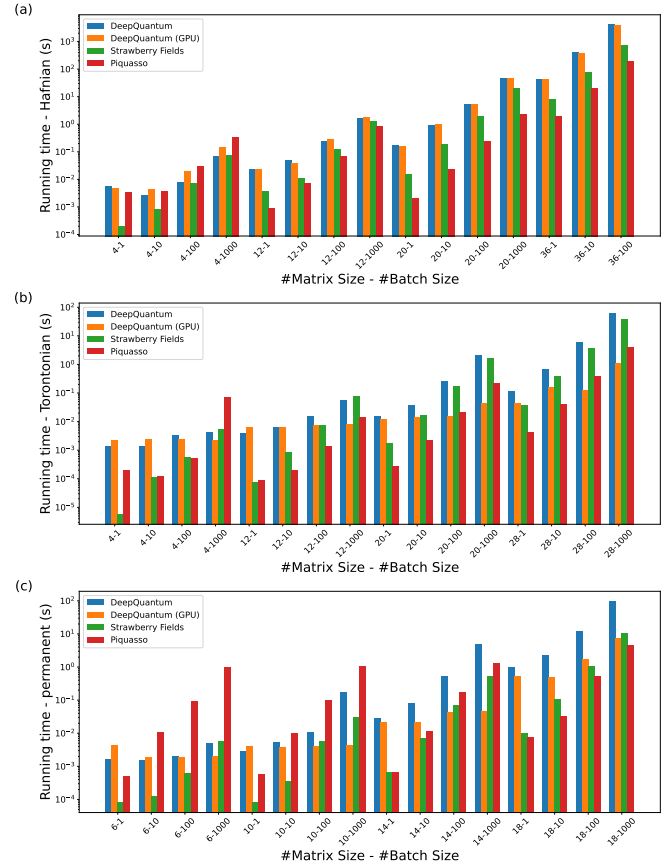


FIG. 3. Benchmark results of Hafnian, Torontonian, and permanent computation between DeepQuantum, Strawberry Fields, and Piquasso.

Benchmark tests were conducted to compare the computational efficiency of Hafnian, Torontonian, and permanent calculations among different quantum computing platforms, including DeepQuantum, Strawberry Fields, and Piquasso. The tests were performed using various matrix sizes and batch sizes, aiming to explore how different systems perform under varying conditions of scale and batch processing.

Fig. 3(a) presents the outcomes of benchmarking the Hafnian calculation methods of DeepQuantum, Strawberry Fields, and Piquasso. Both Piquasso and Strawberry Fields utilize The Walrus interface to achieve highly efficient Hafnian calculations. Conversely, due to the absence of batch processing capabilities in other platforms, DeepQuantum demonstrates competitive performance in small-scale systems, especially with substantial batch sizes. This underscores DeepQuantum's proficiency in managing large batch sizes within smaller quan-

tum systems, illustrating that batch processing can improve performance even when the system scaling is not extensive.

As shown in Fig. 3(b), DeepQuantum (GPU) shows a significant performance boost, outperforming Strawberry Fields and Piquasso under the conditions of large batch sizes and large matrix sizes. This improvement demonstrates the efficiency of Torontonian computations, particularly when the system scale increases.

Fig. 3(c) presents the benchmarking outcomes for computing the permanent. In scenarios involving smaller-scale systems (up to 14 modes), Strawberry Fields, through The Walrus interface, achieves the highest speed in computation. Conversely, for larger-scale systems (18 modes and above), Piquasso surpasses The Walrus in performance, which in turn outperforms DeepQuantum. Nonetheless, provided adequate memory resources, DeepQuantum (GPU) displays minimal sensitivity to fluctuations in batch size, offering enhanced performance in medium-scale applications with large batch sizes (e.g., 10-1000 and 14-1000). This highlights DeepQuantum’s proficiency in effectively managing batch processing at expansive scales.

C. Transpilation and forward computation

We benchmarked the performance of DeepQuantum against Graphix, an open-source library specializing in MBQC simulation, focusing on two representative tasks: pattern transpilation and forward computation [39].

Fig. 4(a) presents the benchmark results for pattern

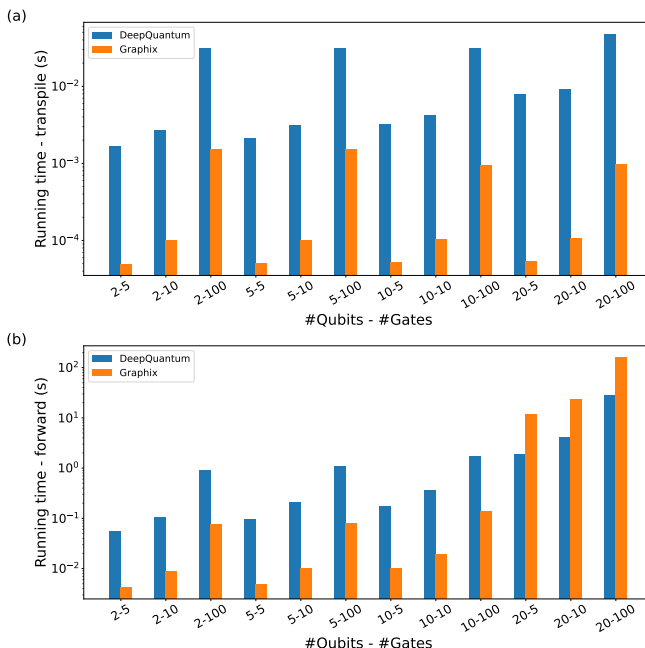


FIG. 4. Benchmark results of pattern transpilation and forward computation between DeepQuantum and Graphix.

transpilation under different numbers of qubits and gates. The translation time for both platforms is extremely short, and thus their impact on the overall task can be regarded as negligible.

Fig. 4(b) reports the benchmark results for the forward computation. Once again, experiments are performed with different numbers of qubits and gates. DeepQuantum exhibits a substantial benefit in terms of execution time when dealing with larger circuits exceeding 20 qubits, indicating its scalability and effectiveness in simulating MBQC.

IV. QUANTUM COMPUTING WITH QUBITS

A. Background

Quantum computing leverages the properties of superposition and entanglement, showing potential in solving certain computational tasks beyond the capabilities of classical computers [4, 40]. Quantum computing uses quantum bits, or qubits, as the fundamental unit of information. A pure state of a qubit can be visualized on the Bloch sphere, parameterized by spherical coordinates θ and ϕ :

$$|\psi(\theta, \phi)\rangle = \cos \frac{\theta}{2} |0\rangle + e^{i\phi} \sin \frac{\theta}{2} |1\rangle, \quad (1)$$

where $|0\rangle \equiv \begin{bmatrix} 1 \\ 0 \end{bmatrix}$ and $|1\rangle \equiv \begin{bmatrix} 0 \\ 1 \end{bmatrix}$ are eigenstates of the Pauli matrix σ_z . Density matrix ρ can also express a quantum state in an orthonormal basis $\{|i\rangle\}$, with elements

$$\rho_{ij} \equiv \langle i | \rho | j \rangle. \quad (2)$$

Quantum gates, represented by unitary matrices U_i , describe operations on qubits. Quantum computation is given by a sequence of quantum gates applied to an initial state

$$|\psi_n\rangle = \prod_{i=1}^n U_i |\psi_0\rangle, \quad (3)$$

or in the density matrix form

$$\rho_n = \prod_{i=1}^n U_i \rho_0 U_i^\dagger, \quad (4)$$

where $\rho_0 = |\psi_0\rangle \langle \psi_0|$ is the initial density matrix, and U_i denotes the i -th unitary gate.

B. API Overview

In DeepQuantum, `QubitCircuit` is the core API for quantum circuit simulation. The entire workflow encompasses the initialization, construction, execution, and measurement of quantum circuits, involving the following four components:

- **Quantum state.** Quantum states are represented by the `QubitState` class, which supports initialization from explicit state vectors and density matrices. Internally, states are stored as `torch.Tensor` objects, enabling native GPU acceleration and seamless integration with PyTorch-based workflows.

- **Quantum operation.** DeepQuantum provides a comprehensive library of quantum operations, including all common fixed and parameterized quantum gates, as well as single-qubit quantum channels. Users can construct a quantum circuit by simply adding these operations to a `QubitCircuit`, specifying the target qubits and corresponding parameters.

- **Quantum circuit.** `QubitCircuit` serves as the core abstraction for simulating quantum circuits. A circuit is initialized with a specified number of qubits and an optional initial quantum state. Quantum operations can then be appended sequentially to define the computational process. The time evolution of the quantum state is implemented via the `forward()` function, which applies all quantum operations in sequence to obtain the final state. Additionally, DeepQuantum offers built-in functions for circuit visualization, compilation, and advanced representations such as matrix product states (MPS) [41].

- **Measurement.** To extract information from evolved quantum states, DeepQuantum supports sampling-based measurement via `QubitCircuit.measure()`, and expectation value evaluation via `QubitCircuit.expectation()`. Observables must be predefined and added to the circuit prior to execution using `QubitCircuit.observable()`.

Collectively, these components form a unified framework that allows users to construct quantum algorithms flexibly and efficiently. Since variational parameters can be natively encoded into a `QubitCircuit`, these methods are essential for VQAs and other hybrid quantum-classical workflows.

Code 1. An illustrative example of `QubitCircuit`

```

1 import deepquantum as dq
2 # Prepare the encoded data
3 data = torch.tensor([1., 2., 3.])
4 # Initialize a 3-qubit circuit
5 cir = dq.QubitCircuit(3)
6 # Add a Hadamard gate
7 cir.h(wires=0)
8 # Add CNOT gates
9 cir.cnot(control=0, target=1)
10 cir.x(wires=2, controls=0)
11 # Add Ry gates to encode data
12 cir.rylayer(encode=True)
13 # Add a layer of CNOT gates in a cyclic way
14 cir.cnot_ring()

```

```

15 # Add Ry gates with variational parameters
16 cir.rylayer()
17 # Set the observable to be measured
18 cir.observable(wires=[0,1,2], basis='xzx')
19 # Execute the circuit via forward()
20 cir(data)
21 # Print the measurement results
22 print(cir.measure(shots=1000, with_prob=True,
23                   wires=[0]))
24 # Print the expectation values
25 exp = cir.expectation()
26 print('Expectation values:')
27 print(exp)
28 # Print the gradients
29 exp.backward()
30 print('Gradients:')
31 for param in cir.parameters():
32     print(param.grad)
33 # Draw the circuit
34 cir.draw()

```

Output:

```

{'0': (850, tensor(0.8387,
grad_fn=<SelectBackward0>)),
'1': (150, tensor(0.1613,
grad_fn=<SelectBackward0>))}
Expectation values:
tensor([0.2592], grad_fn=<StackBackward0>)
Gradients:
tensor(0.2225)
tensor(0.6533)
tensor(0.5036)

```

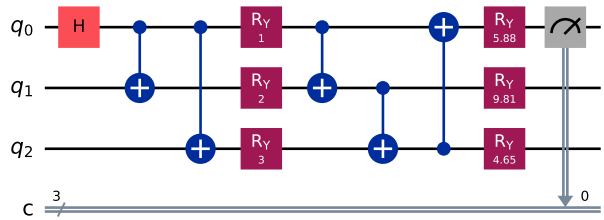


FIG. 5. Visualization of a `QubitCircuit` instance.

Code 1 illustrates a representative example of using `QubitCircuit`. As shown, the framework natively supports automatic differentiation through PyTorch, enabling straightforward gradient computation for variational algorithms. Furthermore, `QubitCircuit` inherently supports batch processing, allowing it to be seamlessly and efficiently integrated into end-to-end PyTorch workflows for large-scale quantum-classical simulations.

C. Applications

1. QResNet

Quantum residual network (QResNet) brings the classical deep learning innovation of residual connections into

the quantum computing domain. Classically, ResNet alleviates the problem of vanishing gradients by adding residual connections [42]. In quantum computing, by contrast, adding residual connections serves the purpose of enhancing the expressivity of quantum neural networks [43], as well as mitigating the barren plateau problem in quantum machine learning [44]. It implements

$$\mathcal{R}(\boldsymbol{\theta}) |\psi\rangle = \frac{1}{2} (\mathbb{I} + \mathcal{L}(\boldsymbol{\theta})) |\psi\rangle \quad (5)$$

with one ancilla qubit. We showcase the advantage of QResNet through a curve-fitting task. The core implementation of QResNet is shown below, demonstrating its PyTorch compatibility:

Code 2. QResNet demo.

```

1 import deepquantum as dq
2 from torch.optim import Adam
3 from torch.nn.functional import mse_loss
4
5 # Model Construction
6 class QNN(nn.Module):
7     def __init__(self, residual=False):
8         super().__init__()
9         self.residual = residual
10        self.build_circuit()
11
12    def build_circuit(self):
13        if self.residual:
14            self.qnn = dq.QubitCircuit(2)
15            self.qnn.u3(wires=1)
16            self.qnn.ry(wires=0)
17            # Encode data
18            self.qnn.ry(wires=0, encode=True,
19            controls=1)
20            self.qnn.ry(wires=0)
21            self.qnn.u3(wires=1)
22            # These gates are variational
23            self.qnn.observable(wires=1, basis='z')
24        )
25
26        self.qnn.observable(wires=[0,1],
27        basis='zz')
28    else:
29        self.qnn = dq.QubitCircuit(1)
30        self.qnn.u3(wires=0)
31        # Encode data
32        self.qnn.ry(wires=0, encode=True)
33        self.qnn.u3(wires=0)
34        self.qnn.observable(wires=0, basis='z')
35
36    def forward(self, x):
37        state = self.qnn(data=x)
38        exp = self.qnn.expectation()
39        if self.residual:
40            exp = exp[:, [0]] + exp[:, [1]]
41        return exp / 2
42
43    # Main training loop
44    def train_model(epochs, model, dataset, lr):
45        train_loader, val_loader = get_loader(dataset)
46        opt = Adam(model.parameters(), lr=lr)
47        for epoch in range(epochs):
48            model.train()
49            train_loss_accum = 0.0
50            for x, y in train_loader:
51
52                yhat = model(x)
53                loss = mse_loss(yhat, y)
54                opt.zero_grad()
55                loss.backward()
56                opt.step()
57                train_loss_accum += loss.item()
58
59            model.eval()
60            val_loss_accum = 0.0
61            with torch.no_grad():
62                for x, y in val_loader:
63                    yhat = model(x)
64                    mse = mse_loss(yhat, y)
65                    val_loss_accum += mse.item()
66
67        return model

```

```

47     yhat = model(x)
48     loss = mse_loss(yhat, y)
49     opt.zero_grad()
50     loss.backward()
51     opt.step()
52     train_loss_accum += loss.item()
53
54     model.eval()
55     val_loss_accum = 0.0
56     with torch.no_grad():
57         for x, y in val_loader:
58             yhat = model(x)
59             mse = mse_loss(yhat, y)
60             val_loss_accum += mse.item()
61
62     return model

```

When the curve to be fitted contains frequency components that correspond to individual generator eigenvalues rather than their differences, residual encoding achieves an MSE that is three orders of magnitude lower compared to traditional encoding. The loss function and results are shown in Fig. 6.

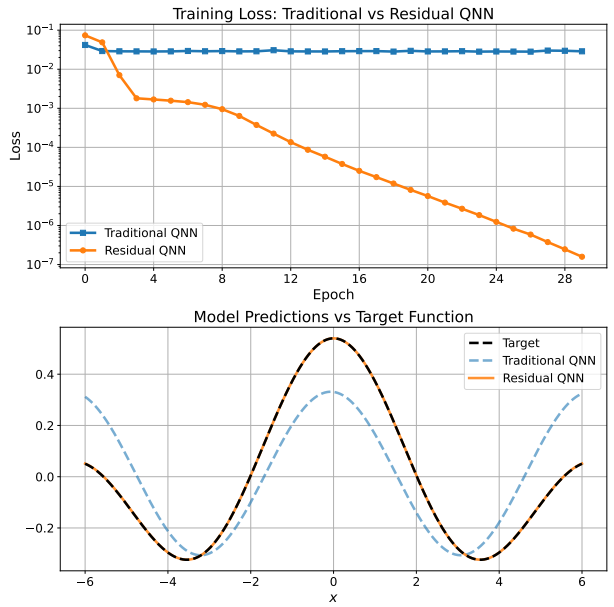


FIG. 6. QResNet training results.

2. QCNN

Quantum convolutional neural network (QCNN) is a hybrid quantum algorithm inspired by classical CNN, which features pooling layers that measure specific qubits and reduce the circuit size, allowing for efficient training and scalability [45]. While initially proposed for quantum state classification [45], QCNN has also been applied to classical tasks [46–48]. We use DeepQuantum to implement image classification based on the MNIST dataset. 12 qubits are used to encode the input image. Our aim is to distinguish between images labeled as 0 and 1, so the sign of the expectation value of the Pauli-Z observable on the last remaining qubit is our classification result.

The core implementation of QCNN is demonstrated below, following ref. [46] as a purely quantum model, to showcase DeepQuantum's support for batch processing and versatile encoding:

Code 3. QCNN demo.

```

1  class QuantumCNN(nn.Module):
2      def __init__(self, nqubit=12):
3          super().__init__()
4          self.nqubit = nqubit
5          self.qc = dq.QubitCircuit(nqubit)
6          self.build_circuit()
7          self.qc.observable(wires=0, basis='z')
8
9      def build_circuit(self):
10         # Encode features hierachically
11         # in between variational gates
12         self.qc.rylayer(encode=True)
13         # 12 encoding gates
14         self.add_conv_layer(12)
15         self.add_pool_layer(12)
16         self.qc.rylayer(wires=range(6), encode=
17             True)
18         self.add_conv_layer(6)
19         self.add_pool_layer(6)
20         self.qc.rylayer(wires=range(3), encode=
21             True)
22         self.add_conv_layer_3qubits()
23         self.add_pool_layer_3to1()
24         # Total 12+6+3=21 encoding gates
25
26         # The following layers are variational
27         def add_conv_layer(self, nqubit):
28             for i in range(0, nqubit - 1, 2):
29                 self.qc.rxx([i, i+1])
30                 self.qc.ryy([i, i+1])
31
32         def add_conv_layer_3qubits(self):
33             for i in range(2):
34                 self.qc.rxx([i, i+1])
35                 self.qc.ryy([i, i+1])
36
36         def add_pool_layer(self, nqubit):
37             for i in range(nqubit // 2):
38                 control = 2 * i + 1
39                 target = 2 * i
40                 self.qc.cry(control, target)
41
41         def add_pool_layer_3to1(self):
42             self.qc.cry(1, 0)
43             self.qc.cry(2, 0)
44
44         # Batch forward pass
45         def forward(self, x):
46             batch_size = x.shape[0]
47             x = x.view(batch_size, 1, 28, 28)
48             features = F.adaptive_avg_pool2d(x, (3,
49                 7))
50             features = features.view(batch_size, -1)
51             angle = np.pi * torch.tanh(features)
52             state = self.qc(data=angle)
53             # Inputs are encoded in batches
54             expectation = self.qc.expectation()
55             output = expectation * 3.0
56             return output.squeeze()

```

Our model achieves a final training accuracy of 94.46%. The loss function history is shown in Fig. 7.

Out of 2115 test samples, the trained model achieves an

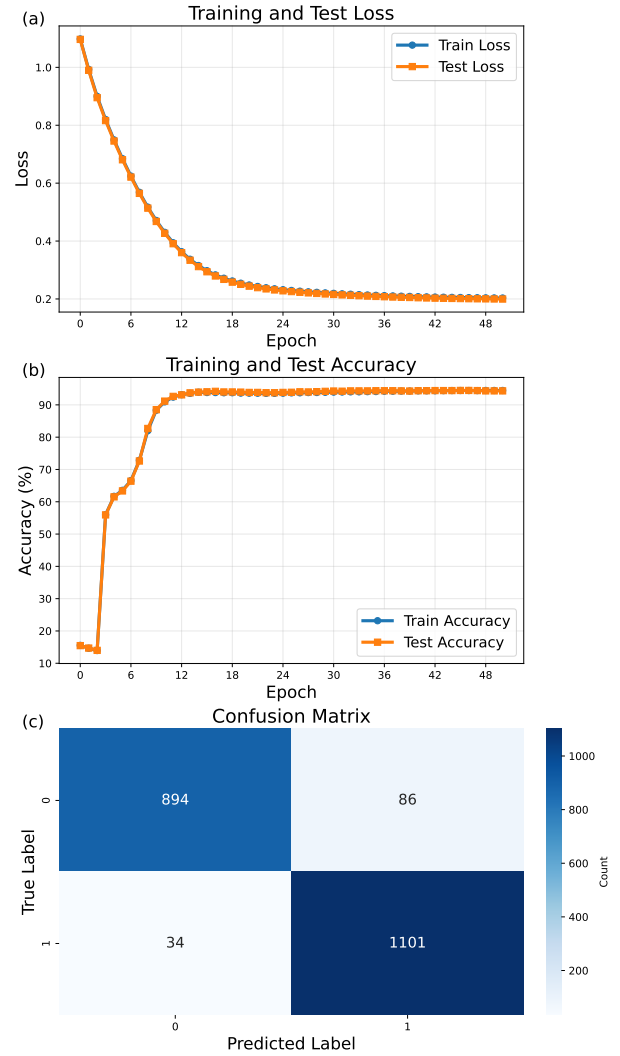


FIG. 7. QCNN training results.

accuracy of 94.33%. The confusion matrix is also shown in Fig. 7.

V. PHOTONIC QUANTUM COMPUTING

A. Background

Photonic quantum computing, which utilizes the properties of photons (such as polarization and coherence), has emerged as a leading candidate for building scalable and efficient quantum processors [49]. Photons, with their low interaction with the environment, allow for relatively robust quantum states that are less susceptible to noise, making them ideal for quantum information processing [50]. Additionally, photons enable the transmission of quantum information over long distances, which is crucial for building quantum networks and integrating quantum computing into real-world applications [51].

Photonic sources are essential for quantum computing and communication, with DV and CV systems being two primary approaches. DV photonic states are encoded in discrete degrees of freedom of light, typical Fock states $|n\rangle$ [52], where $|n\rangle$ is an eigenstate of the photon-number operator \hat{N} :

$$\hat{N}|n\rangle = n|n\rangle. \quad (6)$$

DeepQuantum provides two distinct approaches for simulating DV systems, which correspond to the Fock backend based on basis states and the Fock backend based on state tensors, respectively. One approach models photonic quantum systems as follows, consider an initial N -mode Fock state $\psi_{in} = |n_1, n_2, \dots, n_N\rangle$ incident on an N -mode linear interferometer described by the unitary matrix U , the probability of measuring the output Fock state $\psi_{out} = |m_1, m_2, \dots, m_N\rangle$ is proportional to the squared absolute value of the permanent of a submatrix U_{st} . Specifically, the i -th row of U is repeated n_i times and the j -th column of U is repeated m_i times to form the submatrix U_{st} .

$$|\langle \psi_{out} | \phi(U) | \psi_{in} \rangle|^2 = \frac{|\text{Per}(U_{st})|^2}{n_1! n_2! \dots n_N! m_1! m_2! \dots m_N!}, \quad (7)$$

where $\phi(U)$ represents the action of U on the Fock basis.

The second approach addresses the simulation of systems involving superpositions of Fock states. It employs a tensor representation for the system's evolution, which is a direct generalization of the methods used for multi-qubit systems. In an N -mode system with a local Fock space truncation d , a pure state is a rank- N tensor with shape (d, d, \dots, d) , and the density matrix is represented as a rank- $2N$ tensor. A k -mode photonic quantum gate is a rank- $2k$ tensor. The system's evolution is simulated by applying this gate tensor to the state tensor via tensor contraction over the indices corresponding to the target modes.

In contrast, CV systems utilize continuous properties of light, defined via the canonical mode operators \hat{a} and \hat{a}^\dagger , and commonly visualized in phase space by the quadrature operators [53]:

$$\begin{cases} \hat{x} \equiv \sqrt{\frac{\hbar}{2}}(\hat{a} + \hat{a}^\dagger), \\ \hat{p} \equiv -i\sqrt{\frac{\hbar}{2}}(\hat{a} - \hat{a}^\dagger). \end{cases} \quad (8)$$

The Wigner function provides a powerful phase-space representation of quantum states, serving as a bridge between quantum and classical descriptions. For a single-mode quantum state with density operator ρ , its Wigner function is defined as

$$W(x, p) = \frac{1}{\pi\hbar} \int_{-\infty}^{\infty} \langle x + y | \rho | x - y \rangle e^{-2ipy/\hbar} dy, \quad (9)$$

where x and p denote the position and momentum, or the field quadratures. $W(x, p)$ is a real-valued quasi-probability distribution in phase space, which may

take negative values—signatures of non-classicality in continuous-variable systems. Specifically, the expectation value of an operator \hat{O} can be expressed using the Wigner function.

$$\begin{aligned} \langle \hat{O} \rangle &= \iint W(x, p) O(x, p) dx dp \\ O(x, p) &= 2 \int \langle x + y | \hat{O} | x - y \rangle e^{-2ipy/\hbar} dy \end{aligned} \quad (10)$$

Single-mode Wigner function generalizes naturally to multimode systems. For an m -mode quantum state ρ , the Wigner function is given by the Fourier transform of its characteristic function $\chi_\rho(\eta) = \text{Tr}[\rho, D(\eta)]$:

$$W_\rho(\xi) = \frac{1}{(2\pi)^m} \int_{\mathbb{R}^{2m}} e^{-i\eta^T \Omega \xi} \chi_\rho(\eta) d^{2m} \eta \quad (11)$$

where $\xi = (x_1, x_2, \dots, x_m, p_1, p_2, \dots, p_m)^T$ is the phase-space coordinate vector in the $xxpp$ convention, $D(\eta) = \exp(i\eta^T \Omega \hat{R})$ is the Weyl displacement operator, and the symplectic form is

$$\Omega = \begin{pmatrix} 0 & I_m \\ -I_m & 0 \end{pmatrix}, \quad (12)$$

and the vector of quadrature operators is

$$\hat{R} = (\hat{x}_1, \hat{x}_2, \dots, \hat{x}_m, \hat{p}_1, \hat{p}_2, \dots, \hat{p}_m)^T. \quad (13)$$

This formalism provides a complete description of quantum states in the phase space and is especially convenient for Gaussian states, where the characteristic and Wigner functions take analytic Gaussian forms.

Many fundamental quantum optical components, such as phase shifters and squeezers, implement Gaussian transformations. A transformation is considered Gaussian if it is described by a unitary operator of the form $\hat{U} = \exp(-i\hat{H}/\hbar)$, where the Hamiltonian H is at most quadratic in the quadrature operators. In phase space, the action of such a unitary operator corresponds to a symplectic transformation on the vector of quadrature operators,

$$\hat{U}^\dagger \xi \hat{U} = S \xi + d, \quad (14)$$

where S is a symplectic matrix preserving the symplectic form $S \Omega S^T = \Omega$, d is a displacement vector in phase space.

Gaussian states (like coherent and squeezed states) are commonly used in quantum communication. A Gaussian state is defined as any quantum state whose Wigner function is a Gaussian distribution in the phase space:

$$W_\rho(\xi) = \frac{1}{(2\pi)^m \sqrt{\det V}} \exp\left[-\frac{1}{2}(\xi - d)^T V^{-1}(\xi - d)\right], \quad (15)$$

where $d = \langle \xi \rangle$ is the displacement vector, $V_{ij} = \frac{1}{2}(\xi_i \xi_j + \xi_j \xi_i) - d_i d_j$ is the covariance matrix. In DeepQuantum, a Gaussian state is characterized by the pair (V, d) in

Gaussian backend. Gaussian states form the cornerstone of continuous-variable quantum information protocols, such as quantum key distribution, quantum teleportation, and entanglement distribution [52, 54, 55].

However, universal quantum computation in the CV setting requires the inclusion of non-Gaussian resources, such as photon addition, subtraction, or the preparation of specific non-Gaussian ancilla states [56–59]. DeepQuantum simulates non-Gaussian states ρ whose Wigner function can be written as a linear combination of Gaussian functions in the **Bosonic** backend:

$$W_\rho(\mathbf{r}) = \sum_i w_i G_i(\mathbf{r}), \quad (16)$$

where each $G_i(\mathbf{r})$ is a Gaussian state characterized by its covariance matrix V_i and displacement vector d_i , and w_i are the corresponding complex weights satisfying $\sum_i w_i = 1$. Such a non-Gaussian state is characterized by the pair (V, d, w) .

Two typical non-Gaussian states are the cat state and the GKP state. The cat state is defined as a superposition state of two coherent states:

$$|\text{Cat}\rangle = \frac{1}{\mathcal{N}_\pm} (|+\alpha\rangle + e^{i\phi} |-\alpha\rangle) \quad (17)$$

where $|\alpha\rangle$ is a coherent state $|\alpha\rangle = D(\alpha)|0\rangle$, the even cat state corresponding to $\phi = 0$, and the odd cat state corresponding to $\phi = \pi$. The GKP state [60] is a special quantum error-correcting code that encodes quantum information at specific positions in phase space, forming a regular lattice structure. The general GKP state is defined as

$$|\psi\rangle_{\text{gkp}} = \cos \frac{\theta}{2} |0\rangle_{\text{gkp}} + e^{-i\phi} \sin \frac{\theta}{2} |1\rangle_{\text{gkp}}. \quad (18)$$

Wigner functions of $|0\rangle_{\text{gkp}}$ and $|1\rangle_{\text{gkp}}$ can be expressed as a discrete distribution of Dirac δ functions:

$$W_{\text{gkp}}^0(q, p) = \sum_{s,t=-\infty}^{\infty} (-1)^{st} \delta\left(p - \frac{s\sqrt{\pi\hbar}}{2}\right) \delta\left(q - t\sqrt{\pi\hbar}\right), \quad (19)$$

$$W_{\text{gkp}}^1(q, p) = \sum_{s,t=-\infty}^{\infty} (-1)^{st} \delta\left(p - \frac{s\sqrt{\pi\hbar}}{2}\right) \delta\left(q - (t+1)\sqrt{\pi\hbar}\right). \quad (20)$$

B. API Overview

In DeepQuantum, the central class **QumodeCircuit** is used to simulate photonic quantum circuits. The general simulation workflow consists of four stages: initializing the circuit with quantum states, constructing the circuit by applying gates, evolving the system (performing a forward pass), and finally, sampling results through measurement. Furthermore, to model realistic experimental conditions, noise channels such as photon loss can

be integrated into the circuit. These processes are supported across three distinct backends: **Fock**, **Gaussian** and **Bosonic** backends, as shown in Table III.

TABLE III. Three backends for photonic quantum computing.

Backend	Fock		Gaussian	Bosonic
	based on basis state	based on state vector		
State	Fock basis	State tensor, density matrix	(cov, mean)	(cov, mean, weight)
Detector	PNRD	PNRD, Homodyne	Threshold, Homodyne	Homodyne
Channel	Photon loss	Photon loss	Photon loss	Photon loss

Code 4 and Fig. 8 illustrate a typical workflow, demonstrating the initialization of a multi-mode quantum state, the application of Gaussian operations, circuit evolution, and final measurements via methods such as photon-number or homodyne detection.

The API is organized into several components:

- **Quantum state.** Users can initialize quantum states with different representations, including discrete-variable Fock states, continuous-variable Gaussian states, and non-Gaussian Bosonic states.
- **Quantum operation.** A library of quantum single-mode, two-mode gates and channels is available, such as phase shifter, squeezer, beam splitter, Mach-Zehnder interferometer(MZI), and loss channel.
- **Quantum circuit.** The **QumodeCircuit** class provides methods to assemble gate sequences, execute forward evolution, and visualize circuit structures. Forward propagation (**cir()** or **cir.forward()**) produces the output quantum state, whose data structure depends on the backend.
- **Measurement.** Measurement modules include photon-number-resolving detectors (PNRD), threshold detectors, and homodyne measurements [30]. Different backends support different sampling methods, enabling the extraction of statistical outcomes, probabilities, and quadrature distributions.

Together, these components form a coherent framework that allows users to construct quantum algorithms in a flexible and efficient manner.

Code 4. An illustrative example of **QumodeCircuit**

```

1 import deepquantum as dq
2 import torch
3
4 # Initialize a 2-mode circuit with cutoff=5

```

```

5  cir = dq.QumodeCircuit(2, 'vac', cutoff=5,
6      backend='gaussian')
7
8  # Define trainable parameters
9  r0 = torch.nn.Parameter(torch.tensor(0.5))
10 r1 = torch.nn.Parameter(torch.tensor(1.0))
11
12 # Add squeezing gates
13 cir.s(0, r=r0)
14 cir.s(1, r=r1)
15
16 # Define trainable parameter for beamsplitter
17 theta = torch.nn.Parameter(torch.tensor(1.0))
18 # Add a beamsplitter gate
19 cir.bs([0, 1], inputs=[theta, 1])
20
21 # Forward process
22 cir()
23
24 # Print the measurement results
25 # with different detectors
26 print(cir.measure(shots=100, detector='threshold'))
27 print(cir.measure(shots=100, detector='pnrd'))
28
29 # Set the homodyne measurement on
30 # wire 0 with phase pi/4
31 cir.homodyne(wires=[0], phi=torch.pi/4)
32
33 # Forward process
34 cir()
35
36 # Print the homodyne measurement results
37 sample = cir.measure_homodyne(shots=1024)
38 print(sample)
39
40 # Draw the circuit
41 cir.draw()
42
43 # Forward execution and return
44 # probability distribution with gradients
45 cir(is_prob=True)

```

Output:

```

{|00>: 54, |11>: 31, |01>: 10, |10>: 5}
{|02>: 17, |13>: 15, |04>: 3, |22>: 1, |40>: 1,
 |44>: 2, |20>: 1, |00>: 55, |42>: 5}
tensor([ 1.7850,  2.6191, -0.2665,  ..., 3.1729, -0.5978, -0.1189])
{|00>: tensor([0.5747], grad_fn=<UnbindBackward0>),
 |02>: tensor([0.0714], grad_fn=<UnbindBackward0>),
 |11>: tensor([0.1291], grad_fn=<UnbindBackward0>),
 ...,
 |41>: tensor([0.], grad_fn=<UnbindBackward0>),
 |34>: tensor([0.], grad_fn=<UnbindBackward0>),
 |43>: tensor([0.], grad_fn=<UnbindBackward0>)}

```

Code 4 illustrates a representative example of using `QumodeCircuit`. When using `QumodeCircuit`, we can perform measurements with specific `detectors`, and similar to `QubitCircuit`, it also supports gradient computation and automatic differentiation through PyTorch.

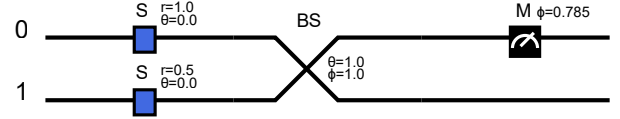


FIG. 8. Visualization of `QumodeCircuit`.

Besides, the Bosonic backend supports initializing non-Gaussian states such as cat states and GKP states, as shown in Code 5.

Code 5. An illustrative example of Bosonic backend

```

1 cir = dq.QumodeCircuit(nmode=2, init_state='vac',
2     backend='bosonic')
3 cir.cat(wires=0, r=1)
4 cir.gkp(wires=1, theta=0, amp_cutoff=0.1)
5 state = cir()
6 for i in state:
7     print(i.shape)

```

Output:

```

torch.Size([1, 1, 4, 4])
torch.Size([1, 356, 4, 1])
torch.Size([1, 356])

```

C. Time-Domain Multiplexing

Photons, serving as flying qubits, can be precisely delayed—a critical capability that enables the time-domain multiplexing (TDM) technique. Leveraging this technique, TDM photonic circuits can generate large-scale, highly entangled CV quantum states, such as cluster states with more than 10,000 entangled modes [61–63]. A canonical time-domain photonic setup is illustrated in Fig. 9. After being squeezed, the $(i+1)$ -th pulse interacts with the loop-internal i -th pulse at a beam splitter. Following the interaction at the beam splitter, the output state is split into two paths. One part is directed back into the delay loop with a phase shifter, where it will interfere with the subsequent incoming pulse. The other part exits the loop and proceeds to the homodyne measurement. Simulating this process requires $(i+1)$ spatial qumodes when implemented using the standard `QumodeCircuit`, which can be both time- and memory-intensive for large i .

To address this, DeepQuantum provides a reconfigurable delay loop. The delay loop, which serves as the core element for TDM, is coupled to the main optical waveguide via a tunable beam splitter, and the path of the loop itself introduces a precise time delay. Critically, embedded within the loop is a phase shifter as shown in Fig. 9.

In `QumodeCircuit`, a delay loop can be added to the circuit via `delay` as shown in Code 6. This method is configured by several parameters, including the `ntau` parameter, which defines the number of qumodes concurrently

stored in the loop, and the `inputs` parameter, which specifies the loop's tunable settings. `QumodeCircuit` only performs a single-step evolution, it provides an `unroll=True` option for visualizing the equivalent single-step spatial circuit (Code 7). For simulating the complete, multi-step dynamics, `QumodeCircuitTDM` should be used. This class handles the full-time evolution and requires that all spatial modes be measured sequentially. A typical example is shown in Code 8. With the `global_circuit` method, the equivalent `QumodeCircuit` can be obtained and visualized. And Fig. 12 shows the equivalent spatial circuit with qumodes `nstep+1`.

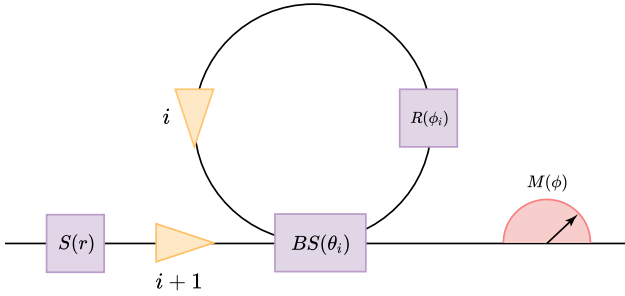


FIG. 9. Time-domain photonic circuit setup.

Code 6. Example of a TDM circuit.

```

1 cir = dq.QumodeCircuit(nmode=1, init_state='vac',
2   cutoff=3)
3 cir.s(0)
4 cir.delay(0, ntau=1, inputs=[torch.pi/4, 0])
5 cir.r(0)
6 cir.homodyne(0)
7 cir.draw()

```

Output:

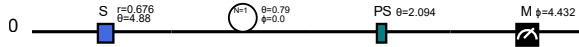


FIG. 10. Time-domain photonic circuit.

Code 7. Equivalent circuit for `QumodeCircuit`.

```

1 cir.draw(unroll=True)

```

Output:



FIG. 11. Equivalent spatial circuit for TDM circuit in Fig. 10.

Code 8. Equivalent circuit for `QumodeCircuitTDM`.

```

1 cir = dq.QumodeCircuitTDM(nmode=1, init_state='vac',
2   cutoff=3)
3 cir.s(0)
4 cir.delay(0, ntau=1, inputs=[torch.pi/4, 0])
5 cir.r(0)
6 cir.homodyne(0)
7 cir_global = cir.global_circuit(nstep=2)
8 cir_global.draw(unroll=True)

```

Output:

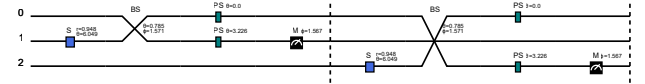


FIG. 12. Equivalent spatial circuit for TDM circuit in Fig. 10.

D. Applications

1. CNOT based on dual-rail encoding

The controlled-NOT (CNOT) gate is a fundamental entangling gate in quantum computing. It plays a pivotal role in universal quantum computation, enabling the generation of entangled states, the implementation of error correction, and the construction of logical circuits. Combined with single-qubit gates, the CNOT gate forms a universal gate set, making it indispensable for the physical realization of a quantum processor [40, 64].

However, in photonic quantum computing platforms, implementing a deterministic CNOT gate remains highly challenging. In contrast to matter-based qubits such as superconducting circuits or trapped ions, photons do not directly interact within linear optical media [65]. To overcome this fundamental challenge, the Knill-Laflamme-Milburn (KLM) protocol was developed [49]. It introduces a method to induce an effective interaction between photons by leveraging projective measurements with photon detectors. A key consequence of this approach is its inherently probabilistic nature, which categorizes it as a non-deterministic model of quantum computation.

In this application, the dual-rail encoding technique [66] is employed to implement the probabilistic CNOT gate within the DV framework. Specifically, each qubit is represented across two modes, with a single photon introduced into the system. The qubit state is then determined by the photon's position within the two waveguides, as illustrated in Fig. 13:

$$\begin{cases} |0\rangle_L = |1\rangle_a \otimes |0\rangle_b, \\ |1\rangle_L = |0\rangle_a \otimes |1\rangle_b. \end{cases} \quad (21)$$

The application of the CNOT gate begins with a probabilistic controlled-Z (CZ) gate. The CNOT gate can be constructed from the CZ gate by applying a Hadamard gate before and after the target qubit [67]:

$$\text{CNOT} = (I \otimes H) \cdot \text{CZ} \cdot (I \otimes H) \quad (22)$$

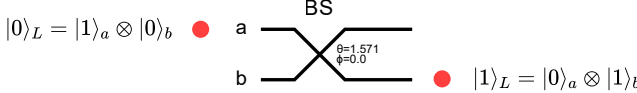


FIG. 13. Definition of dual-rail encoding.

We use a 6-mode photonic circuit to realize the probabilistic CNOT gate in Code 9. As illustrated in Fig. 14, among the six modes, modes 0 and 5 serve as ancilla modes, while modes 1-2 encode the first qubit, and modes 3-4 encode the second qubit using the dual-rail encoding scheme.

$$\begin{cases} |00\rangle_L = |1010\rangle_{1,2,3,4}, \\ |01\rangle_L = |1001\rangle_{1,2,3,4}, \\ |10\rangle_L = |0110\rangle_{1,2,3,4}, \\ |11\rangle_L = |0101\rangle_{1,2,3,4}. \end{cases} \quad (23)$$

Post-selection process is then applied as follows. Only events where the sum of photon numbers in modes 1 and 2 equals 1, and simultaneously the sum of photon numbers in modes 3 and 4 equals 1, are retained. This ensures the preservation of the dual-rail encoded qubit structure throughout the computation. The CNOT gate in this structure has a probability of 1/9, as invalid quantum states are removed through post-selection.

Code 9. Example of photonic CNOT gate.

```

1 import deepquantum as dq
2 import torch
3 # the first and last modes are ancilla modes
4 init_state = [0, 1, 0, 1, 0, 0]
5 cir = dq.QumodeCircuit(6, init_state)
6 theta = torch.acccos(torch.tensor(1/3 ** 0.5)) *
7     2
8 # Hadamard gate
9 cir.h([3,4])
10 # CZ gate
11 cir.ps(1, torch.pi)
12 cir.bs_h([0,1], theta)
13 cir.ps(0, torch.pi)
14 cir.ps(3, torch.pi)
15 cir.bs_h([2,3], theta)
16 cir.ps(2, torch.pi)
17 cir.bs_h([4,5], theta)
18 # Hadamard gate
19 cir.h([3,4])
20 print('|00>->|00> amplitude:')
21 print(
22     cir.get_amplitude(
23         final_state=[0, 1, 0, 1, 0, 0],
24         init_state=[0, 1, 0, 1, 0, 0],
25     )
26 )
27 print('|01>->|01> amplitude:')
28 print(
29     cir.get_amplitude(
30         final_state=[0, 1, 0, 0, 1, 0],
31         init_state=[0, 1, 0, 0, 1, 0],
32     )
33 )
34 print('|10>->|11> amplitude:')

```

```

34 print(
35     cir.get_amplitude(
36         final_state=[0, 0, 1, 0, 1, 0],
37         init_state=[0, 0, 1, 1, 0, 0],
38     )
39 )
40 print('|11>->|10> amplitude:')
41 print(
42     cir.get_amplitude(
43         final_state=[0, 0, 1, 1, 0, 0],
44         init_state=[0, 0, 1, 0, 1, 0],
45     )
46 )
47 cir.draw()

```

Output:

```

|00>->|00> amplitude:
tensor([0.3333+4.3711e-08j])
|01>->|01> amplitude:
tensor([0.3333+4.3711e-08j])
|10>->|11> amplitude:
tensor([0.3333+4.3711e-08j])
|11>->|10> amplitude:
tensor([0.3333+4.3711e-08j])

```

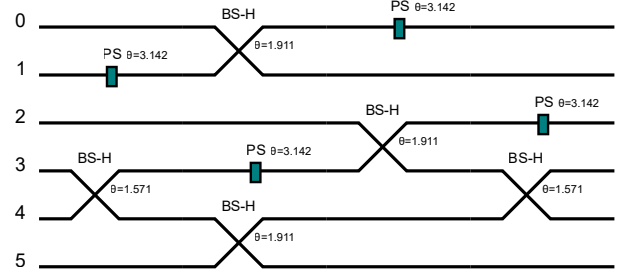


FIG. 14. Structure of CNOT gate in DeepQuantum visualization.

2. Unitary transformation with Clements structure

Linear optical quantum computing (LOQC) relies on the precise implementation of arbitrary unitary transformations across multiple photonic modes [68–72]. One of the most efficient and compact approaches is the Clements architecture [72], which enables the decomposition of any unitary matrix into a structured sequence of optical components such as beam splitters and phase shifters.

Code 10 illustrates an example of a 6-mode Clements structure. Class `UnitaryDecomposer` decomposes the unitary matrix into parameters corresponding to Clements structure. Here `u` requires to be a unitary matrix. The parameters can be encoded into the Clements structures by the `dict2data` method. Fig. 15 shows its structures and all the parameters for beam splitters and phase shifters.

Code 10. Example of clements structure.

```

1 import deepquantum as dq
2 import torch
3
4 u = torch.tensor(
5     [[1, 0, 1, -1, 0, 0],
6      [0, 1, 0, 0, 0, 2 ** 0.5],
7      [1, 0, 0, 1, 1, 0],
8      [-1, 0, 1, 0, 1, 0],
9      [0, 0, 1, 1, -1, 0],
10     [0, 2 ** 0.5, 0, 0, 0, -1]]) / 3 ** 0.5
11
12 # Decompose the unitary matrix into
13 # parameters corresponding to Clements
14 ud = dq.UnitaryDecomposer(u)
15 angle_dict = ud.decomp()[2]
16 clements = dq.Clements(nmode=6, init_state
17 = [1, 0, 1, 0, 0, 0], cutoff=3)
18
19 # Encode the line parameters into
20 # the 6 times 6 Clements architecture
21 data = clements.dict2data(angle_dict)
22 state = clements(data=data)
23 clements.draw()

```

Output:

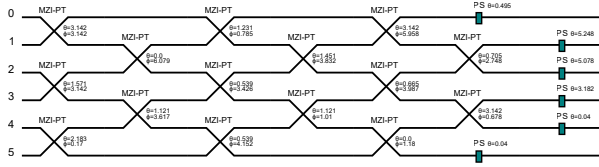


FIG. 15. Visualization of equivalent Clements structure circuit.

3. Gaussian Boson sampling

Gaussian Boson Sampling is a quantum computational model that leverages the quantum properties of light to address complex sampling problems [30, 73]. In GBS, squeezed vacuum states of photons are injected into a linear optical interferometer and measured in the Fock basis. The task of sampling from the output distribution of a GBS device is widely believed to be classically intractable. This computational hardness establishes GBS as a prime candidate for demonstrating quantum advantage [3, 30, 74–76]. Furthermore, GBS offers a significant advantage for solving problems that can be directly encoded into its architecture, such as molecular docking [77], graph similarity [78], and finding maximum cliques [79].

DeepQuantum provides an intuitive interface for the direct construction of GBS circuits via `GaussianBosonSampling` class, where users can define the squeezing parameters and the linear optical interferometer. Furthermore, it offers a higher-level abstraction for tackling graph-relevant problems via `GBS_Graph` class. This functionality streamlines the

process by automatically encoding a graph's structure into the GBS circuit and subsequently performing the sampling.

Code 11 illustrates the construction of a GBS circuit `GaussianBosonSampling`. Six modes are initialized with single-mode squeezing operations and propagated through an identity interferometer. Subsequently, method `measure()` implements the measurement operations. Photon number resolving detectors and threshold detectors are provided for Fock basis measurement, corresponding to `detector='pnrnd'` and `detector='threshold'` in `measure()` method.

Code 11. Example of GBS with build-in method.

```

1 import deepquantum as dq
2 import numpy as np
3
4 # Define squeezing parameters and unitary
5 # transformation
6 squeezing = [1] * 6
7 unitary = np.eye(6)
8
9 # Initialize the GBS circuit
10 gbs = dq.GaussianBosonSampling(nmode=6, squeezing
11     = squeezing, unitary=unitary)
12
13 # Build and visualize the circuit
14 gbs()
15
16 # Draws the sampling circuit
17 gbs.draw()
18
19 result = gbs.measure(shots=1024, detector='pnrnd')
20 print('pnrnd:', result)
21
22 result = gbs.measure(shots=1024, detector='threshold')
23 print('threshold:', result)

```

Output:

```

pnrnd:{|202020>: 2, |022220>: 3, ...}
threshold:{|100100>: 41, |101101>: 15, ...}

```

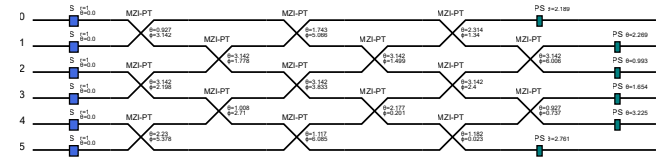


FIG. 16. Structure of GBS circuit.

The `GBS_Graph` class encodes graph information into a GBS device. This is achieved by first decomposing the graph's adjacency matrix, and then mapping the resulting components onto the required squeezing parameters and the interferometer's parameters [80, 81].

Code 12 illustrates a GBS setup based on a six-node graph. Similar to `QumodeCircuit`, the `GBS_Graph` class allows for the evolution of the circuit followed by measurement. The `measure()` method returns a dictionary in which each key corresponds to a sampled Fock state,

and each value denotes the number of occurrences of that state.

Code 12. GBS graph setup and measurement.

```

1 import deepquantum.photonic as dqp
2 import torch

3

4 # Define the adjacency matrix of the graph
5 adj_mat = torch.tensor([
6     [0., 1., 1., 0., 0., 0.],
7     [1., 0., 0., 1., 0., 1.],
8     [1., 0., 0., 0., 0., 0.],
9     [0., 1., 0., 0., 1., 1.],
10    [0., 0., 0., 1., 0., 0.],
11    [0., 1., 0., 1., 0., 0.]]

12

13 # Initialize the GBS circuit with cutoff 2
14 gbs = dqp.GBS_Graph(adj_mat=adj_mat, cutoff=2)
15

16 # Build the GBS state
17 state = gbs()
18

19 # Perform sampling
20 sample = gbs.measure()
21 print(sample)

```

Output:

{|000011>: 1, |101011>: 2, ...}

4. Preparation of EPR state with TDM

Quantum entanglement is a fundamental resource for quantum information processing, both in DV and CV systems. Among the most widely used entangled states are the Einstein-Podolsky-Rosen (EPR) states [82] and Greenberger-Horne-Zeilinger (GHZ) states [83], both of which play crucial roles in quantum communication and quantum networking [52, 84].

A significant breakthrough was achieved by the Furusawa group, whose TDM scheme based on optical delay loops allowed for the flexible generation of entangled states like EPR and GHZ [61, 85]. This work established the foundation for producing large-scale one- and two-dimensional cluster states, a pivotal advance toward universal quantum computation [86, 87].

The EPR state can be described in the quadrature x basis as follows,

$$|EPR\rangle_{AB} \sim \int_{-\infty}^{+\infty} |x_0\rangle_x^A |x_0\rangle_x^B dx_0. \quad (24)$$

Thus, when a homodyne measurement on mode A yields outcome x_0 , mode B will also yield the same outcome x_0 .

The TDM circuit of an EPR entangled state generation is shown in Fig. 17. The parameters of the delay loop are set as $[\pi/2, \pi/2]$ to swap the initial vacuum state out of the loop. Subsequently, the parameters are switched to $[\pi/4, 0]$, which allows for the interference of two consecutive squeezed coherent states to create an EPR pair. This

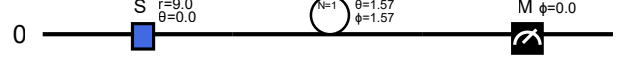


FIG. 17. Two-mode circuit for EPR state preparation.

process is then repeated iteratively to produce a sequence of entangled EPR states.

The realization using DeepQuantum is shown in Code 13.

Code 13. Simulation of EPR state preparation.

```

1 import deepquantum as dq
2 import torch
3
4 r = 9
5 nmode = 1
6 cir = dq.QumodeCircuitTDM(nmode=nmode, init_state
7     ='vac')
8 cir.s(0, r=r)
9 cir.delay(0, ntau=1, inputs=[torch.pi/2,torch.pi
10    /2], encode=True)
11 cir.homodyne_x(0)
12 data = torch.tensor([[torch.pi/2,torch.pi/2],
13     [torch.pi/4, 0]]).unsqueeze
14 (0)
15 cir(data=data, nstep=13)
16 cir.samples[1:]

```

Output:

tensor([4112.4751, 4112.4751,
-5751.3506, -5751.3506,
-6159.6787, -6159.6787,
526.8242, 526.8240,
-6301.3857, -6301.3857,
-5215.0078, -5215.0078])

5. Preparation of two-dimensional cluster state with TDM

The experimental realization of a two-dimensional cluster state was reported in ref. [61], achieved through the generation of continuous-variable entanglement in a four-mode photonic circuit featuring two delay loops, as illustrated in Fig. 18.

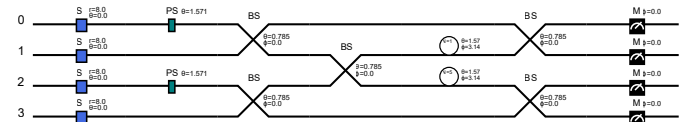


FIG. 18. Schematic of the four-mode entangling circuit.

The process begins with the generation of four squeezed photonic modes. At each time step, these modes are directed into a network of three 50 : 50 beam splitters, where they interfere to generate entanglement. Following this interaction, mode 1 is routed through a delay loop corresponding to a single time period (τ), while

mode 2 undergoes a significantly longer delay of N periods ($N\tau$), with $N = 5$ in the experiment. This procedure yields a final entanglement state in both the temporal and spatial domains. The resulting cluster state is characterized by the nullifier relation:

$$x_k^A + x_k^B - \frac{1}{\sqrt{2}}(-x_{k+1}^A + x_{k+1}^B + x_{k+N}^C + x_{k+N}^D) = 0, \quad (25)$$

where k indexes the time steps, A, B, C, D correspond to 4 distinct modes.

The TDM circuits can be unrolled into spatial circuits. The equivalent spatial circuit is shown in Fig. 19 with `nstep=1`.

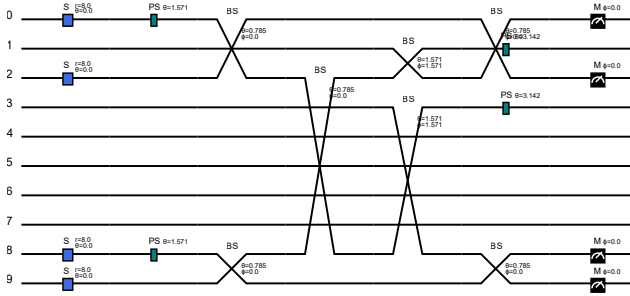


FIG. 19. Equivalent spatial circuit.

A numerical simulation of the preparation process is given in Code 14.

Code 14. Simulation of cluster state preparation.

```

1 import deepquantum as dq
2 import numpy as np
3 import torch

4
5 cir = dq.QumodeCircuitTDM(4, 'vac', 3)
6 for i in range(4):
7     cir.s(i, r=8)
8 cir.r(0, np.pi/2)
9 cir.r(2, np.pi/2)
10 cir.bs([0,1], [np.pi/4, 0])
11 cir.bs([2,3], [np.pi/4, 0])
12 cir.bs([1,2], [np.pi/4, 0])
13 cir.delay(1, ntau=1, inputs=[np.pi/2, np.pi])
14 cir.delay(2, ntau=5, inputs=[np.pi/2, np.pi])
15 cir.bs([0,1], [np.pi/4, 0])
16 cir.bs([2,3], [np.pi/4, 0])
17 for i in range(4):
18     cir.homodyne_x(i)
19 cir.to(torch.double)
20 cir()
21 cir.draw()

```

To confirm the correctness of the simulation, we evaluate the nullifier in Eq. (25) over 100 time steps in Code 15. The variance and mean of the residuals are found to be close to zero, consistent with the expected cluster state.

Code 15. Verification of cluster state preparation.

```

1 cir(nstep=100)
2 samples = cir.samples.mT
3 err = []

```

```

4 for i in range(90):
5     temp = samples[i][2].sum()
6     - 1 / np.sqrt(2) * (-samples[i+1][0]
7     + samples[i+1][1]
8     + samples[i+5][2].sum())
9     err.append(temp)
10 err = torch.tensor(err)
11 print('variance:', err.std()**2)
12 print('mean:', err.mean())

```

variance: tensor(5.4542e-07, dtype=torch.float64)
mean: tensor(-3.7434e-05, dtype=torch.float64)

6. Generation of Non-Gaussian GKP state

Non-Gaussian states are extremely important resources in quantum information processing, playing a crucial role in enabling nonlinearity, quantum error mitigation, and quantum advantage in photonic systems. Unlike Gaussian states whose Wigner functions are strictly positive, non-Gaussian states exhibit negative regions in their Wigner functions, serving as clear signatures of quantum nonclassicality. A special case is the GKP state, which is proposed as an error correction protocol.

A finite-energy GKP state [88, 89] can be regarded as a Fock damping operator $e^{-\epsilon\hat{n}}$ acting on the ideal case, forming a superposition of multiple Gaussian wave packets, with a Gaussian envelope, as illustrated in Fig. 20.

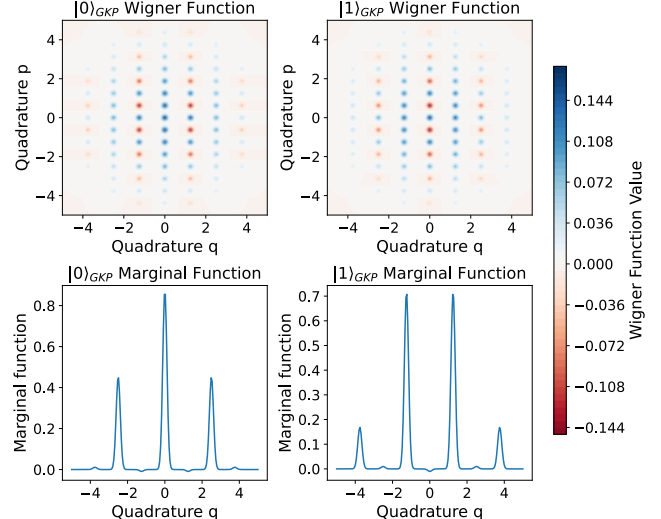


FIG. 20. Wigner function of finite-energy GKP states.

GKP states have already been prepared experimentally through breeding [22] and the post-selection method [21]. In the breeding approach, two squeezed cat states are injected into two modes and entangled with a beam splitter, and then a homodyne measurement is implemented on the first mode, with results close to 0 selected. This process is the first breeding. In subsequent breedings, the output states from previous ones are injected as inputs.

The output GKP state features more lattice structure as the number of breeding times grows. We jointly demonstrate a two-breeding, including the quantum operations and Wigner functions for input and output states, in Fig. 21.

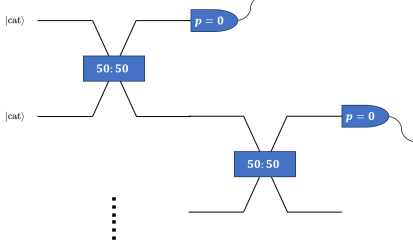


FIG. 21. Diagram of experimentally preparing GKP states by breeding twice.

Code 16. First breeding.

```
# First breeding
r = 1.5
alpha = torch.tensor(2, dtype=torch.double)
alpha_prime = (np.cosh(r) + np.sinh(r)) * alpha /
    2
cir = dq.QumodeCircuit(nmode=2, init_state='vac',
    backend='bosonic')
# Plus cat state
cir.cat(wires=0, r=alpha_prime, theta=0, p=0)
# Plus cat state
cir.cat(wires=1, r=alpha_prime, theta=0, p=0)
cir.s(0, r)
cir.s(1, r)
cir.bs(wires=[0,1], inputs=[np.pi/4, 0])
cir.homodyne_p(wires=0)
cir.to(torch.double)
state = cir()
sample = cir.measure_homodyne(shots=5000)
% cir.draw()
```

Code 17. Select close-to-zero measurement results.

```
# For reproducibility, select results
# where the measurement value is close to 0
for i in range(len(sample)):
    if abs(sample[i]) < 0.001:
        k = i
        print(i, sample[i])
idx = torch.tensor([1, 3])
bs_lst = [
    cir.state_measured[0][k][..., idx[:, None],
        idx],
    cir.state_measured[1][k][..., idx, :],
    cir.state_measured[2][k]
]
stateCollapse = dq.BosonicState(bs_lst, nmode=1)
wigner = stateCollapse.wigner(wire=0)
```

4632 tensor(0.0002, dtype=torch.float64)

Code 18. Second breeding.

```
# Second breeding
cir2 = dq.QumodeCircuit(nmode=2, init_state=[state,
    collapse, state_collapse], backend='bosonic')
cir2.bs(wires=[0,1], inputs=[np.pi/4, 0.])
cir2.homodyne_p(wires=0)
cir2.to(torch.double)
state2 = cir2()
sample2 = cir2.measure_homodyne(shots=1000)

for i in range(len(sample2)):
    if abs(sample2[i]-0) < 0.002:
        k = i
        print(i, sample2[i])
idx = torch.tensor([1, 3])
bs_lst2 = [
    cir2.state_measured[0][k][..., idx[:, None],
        idx],
    cir2.state_measured[1][k][..., idx, :],
    cir2.state_measured[2][k]
]
state_collapse2 = dq.BosonicState(bs_lst2, nmode=1)

wigner = state_collapse2.wigner(wire=0)
```

148 tensor(-0.0016, dtype=torch.float64)
201 tensor(-0.0004, dtype=torch.float64)

The diagram of the post-selection method is shown in Fig. 22. Four squeezed vacuum states are injected into an interferometer U_G composed of beam splitters and phase shifters. Photon number resolving detection is implemented on modes 1-3, and the results are (m_1, m_2, m_3) . The output state on mode 0 will be a GKP state by choosing the proper (m_1, m_2, m_3) and U_G .

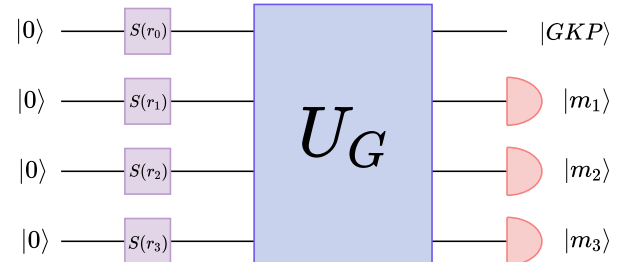


FIG. 22. Diagram of experimentally preparing GKP states by post-selection.

Code 19 shows an example of GKP state $|0\rangle$ preparation by the post-selection method with the Gaussian boson sampling circuit. The preparation circuit is shown in Fig. 23, and the Wigner function and marginal function are shown in Fig. 24.

Code 19. Example of GKP state $|0\rangle$ preparation by post-selection.

```
1 import deepquantum as dq
2 import torch
```

```

3
4 nmode = 4
5 cutoff = 50
6
7 cir = dq.QumodeCircuit(nmode=nmode, init_state='vac', cutoff=cutoff, backend='fock', basis=False)
8
9 # squeeze vacuum states
10 squeeze = [1.0678, 0.9997, 1.1976, 0.8253]
11 for i in range(nmode):
12     cir.s(wires=i, r=squeeze[i])
13
14 # unitary operations
15 theta = [2.4144, 0.4863]
16 cir.ps(wires=1, inputs=np.pi/2)
17 cir.ps(wires=2, inputs=np.pi/2)
18 cir.ps(wires=3, inputs=np.pi/2)
19 cir.bs(wires=[0,1], inputs=[theta[0], 0])
20 cir.bs(wires=[1,2], inputs=[theta[1], 0])
21 cir.bs(wires=[2,3], inputs=[torch.pi/4, 0])
22 cir.ps(wires=0, inputs=np.pi/2)
23 state = cir()
24
25 # post-selection measurement
26 select = [4, 2, 4]
27 state0 = state[0, :, select[0], select[1], select[2]]
28 state0 = state0 / torch.sum(torch.abs(state0)**2)
29     **0.5
30
31 # plot Wigner function, marginal function
32 .....
33 cir.draw('GKP-post-selection-circuit.svg')

```

Output:

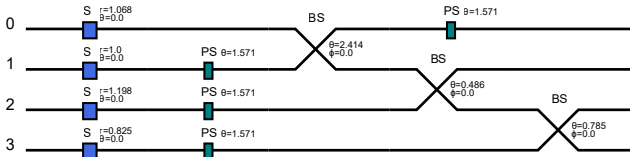


FIG. 23. GKP state $|0\rangle$ preparation circuit.

VI. MEASUREMENT-BASED QUANTUM COMPUTING

A. Background

Measurement-based quantum computing uses cluster or graph states as resources, and operations are conducted as a sequence of measurements on certain nodes. Each measurement outcome determines the basis of subsequent measurements and Pauli corrections, enabling information flow [90, 91]. MBQC can be conveniently implemented on photonic devices [92, 93], and has been applied in universal quantum algorithms [94], fault-tolerant quantum computing [95–97], and blind quantum computing [98, 99].

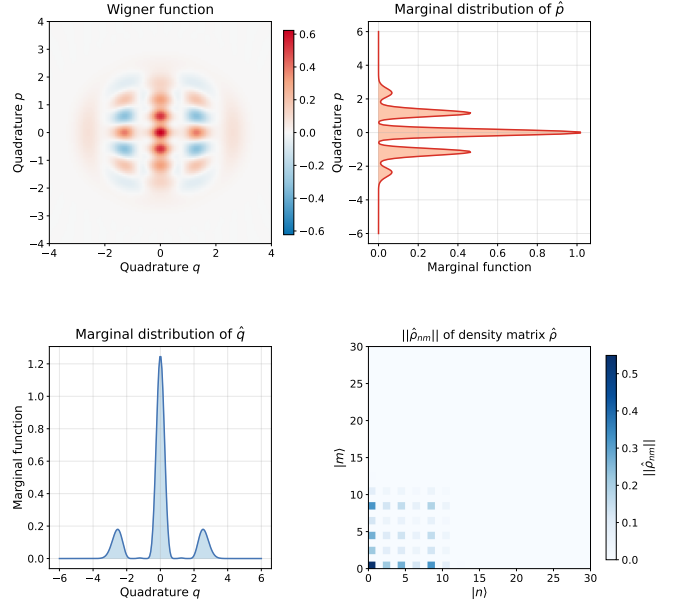


FIG. 24. Wigner function, marginal distribution of GKP state $|0\rangle_{\text{GKP}}$, and $\|\hat{\rho}_{nm}\|$ (norm of element (n, m) of its density matrix), prepared by post-selection.

B. API Overview

DeepQuantum provides a comprehensive MBQC framework, featuring its construction, conversion, execution, optimization, and visualization, as elaborated below. It centers on the `Pattern` class.

- **Construction from scratch.** An MBQC pattern is characterized by commands on a graph state. The graph state is constructed by the method `n(i)`, which initializes node i , and `e(i,j)`, which applies a CZ entanglement between nodes i and j . `m(i,alpha,lambda,t,s)` indicates measuring node i on the $\lambda \in \{XY, YZ, ZX\}$ plane at angle α , modified by feedforward domains s and t . Finally, `x(i,s)` and `z(i,s)` specify X and Z corrections on node i based on domain s .
- **Transpilation.** Alternatively, an MBQC pattern can be transpiled from a `QubitCircuit` by calling `QubitCircuit.pattern()`. The resulting `Pattern` is a ‘wild’ one in the sense that mid-circuit corrections are not absorbed into measurement angles.
- **Standardization / Optimization.** Standardization is implemented as `Pattern.standardize()`. It merges mid-circuit corrections with measurement angles, which removes the need for physical conditional gates and enables a purely measurement-driven implementation. Optimization via `Pattern.shift_signals()` serves to remove the dependencies of measurement angles on the `t` domain, reducing quantum depth.

• Execution / Forward.

Calling `Pattern.forward()` yields the output of MBQC as a `GraphState` class, while its `full_state` attribute returns a normalized state vector for qubits, with dimension corresponding to the number of unmeasured nodes.

The complete workflow for MBQC involves constructing a `Pattern`, standardizing and optimizing the pattern, and executing it.

Code 20. MBQC pattern workflow.

```

1 # Initialization
2 pattern = dq.Pattern(nodes_state=[0, 1])
3 # Add nodes
4 pattern.n(2)
5 # Add edges
6 pattern.e(0, 2)
7 pattern.e(1, 2)
8 # Add measurements
9 pattern.m(node=0, angle=np.pi)
10 pattern.m(node=1, angle=np.pi, s_domain=[0])
11 pattern.n(3)
12 pattern.e(2, 3)
13 pattern.m(node=2, angle=np.pi, s_domain=[0],
14 t_domain=[1])
15 # X correction
16 pattern.x(node=3, domain=[0, 1])
17 # Standardization & Optimization
18 pattern.standardize()
19 pattern.shift_signals()
20
21 # Visualization
22 pattern.draw()

```

The outputs from with (right) or without (left) the line `pattern.shift_signals()` are shown in Fig. 25.

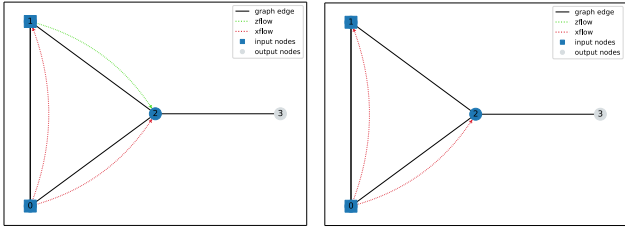


FIG. 25. MBQC pattern visualization.

Alternatively, a `Pattern` can be transpiled from a `QubitCircuit`, followed by standardizing, optimizing, and execution.

Code 21. MBQC transpilation workflow.

```

1 # Construct a qubit circuit
2 circuit = dq.QubitCircuit(2)
3 circuit.h(0)
4 circuit.h(1)
5 circuit.cnot(0, 1)
6 circuit.draw()
7
8 # Transpile to a pattern
9 pattern = circuit.pattern()
10 pattern.standardize()

```

```

11 pattern.shift_signals()
12 pattern.draw()

```

We also compare the original `QubitCircuit` and transpiled `Pattern` in Fig. 26.

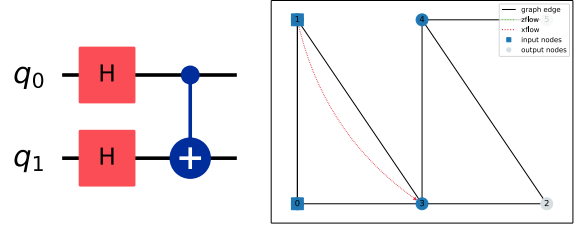


FIG. 26. MBQC transpilation comparison.

C. Applications

In DeepQuantum, a variational qubit circuit can be transpiled into a variational MBQC pattern that preserves auto-differentiation. In addition, data can be encoded to measurement angles using the `encode=True` flag. Batch inputs and data re-uploading are also supported. Below, we train a quantum classifier whose qubit circuit ansatz employs data-reuploading, with data encoded repeatedly. Data re-uploading allows fewer qubits and shallower circuits to perform complex tasks. The classifier implements binary classification on a non-linearly separable circles dataset. Input data contains two features, which are zero-padded to three to accommodate three rotation gates. In layer i out of 4 layers, the variational parameters θ_i , later transpiled into the MBQC pattern, are given by

$$\theta_i = \beta_i + \alpha_i \odot \vec{x}, \quad (26)$$

where α_i, β_i are trainable parameters, \odot represents element-wise multiplication, and the features \vec{x} are re-uploaded across different layers. We minimize the MSE loss

$$\mathcal{L} = \frac{1}{N} \sum_{i=1}^N \left| y^{(i)} - \langle Z \otimes Z \rangle_{\theta}^{(i)} \right|^2. \quad (27)$$

The loss function history and final decision boundary are shown below, demonstrating the auto-differentiation advantages of DeepQuantum relative to Graphix, a non-auto-differentiating package.

VII. LARGE-SCALE SIMULATIONS

A. Tensor Network and Matrix Product State

Tensor network provides a powerful solution to the exponentially large complexity with respect to a large-scale

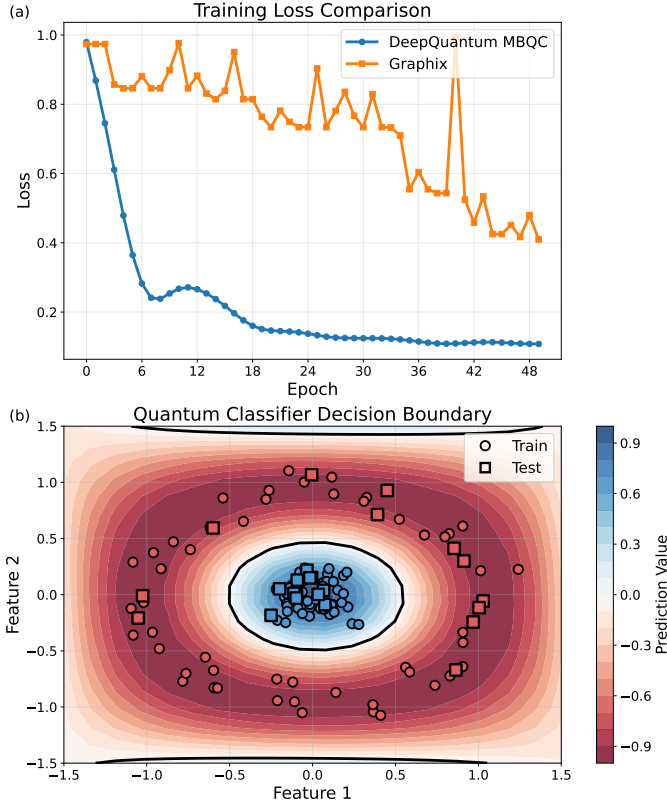


FIG. 27. MBQC training results with reuploading.

quantum circuit, in terms of its simulation [100–103], optimization [104, 105], and entanglement analysis [106–108].

A tensor can be represented as a multidimensional array of numbers in a specific basis. Components of a $d_1 \times d_2 \times \dots \times d_r$ -dimension tensor can be expressed as

$$T_{i_1, i_2, \dots, i_r} \in \mathbb{C}^{d_1 \times d_2 \times \dots \times d_r}. \quad (28)$$

Here, each index i_k can take values from 1 to d_k , where d_k is the dimension of that index, and r is the rank of the tensor. Scalars, vectors, and matrices are rank-0, rank-1, and rank-2 tensors, respectively. In Penrose tensor diagram [109], an r -th rank tensor is represented as a block with r legs (lines) emerging from it. Each leg corresponds to one of the tensor's indices.

The fundamental operation within a tensor network is contraction, which generalizes matrix multiplication. A contraction involves summing over one or more shared indices between two or more tensors, and is expressed in a tensor diagram by joining two legs corresponding to the index summed over.

In Fig. 28, the diagrams for matrix trace, matrix multiplication, and more complex tensor contractions are illustrated.

The primary challenge in simulating large quantum systems is the so-called “curse of dimensionality”. The Hilbert space for a system of N qubits grows exponentially with N . The state of N qubits $|\psi\rangle$ is described by

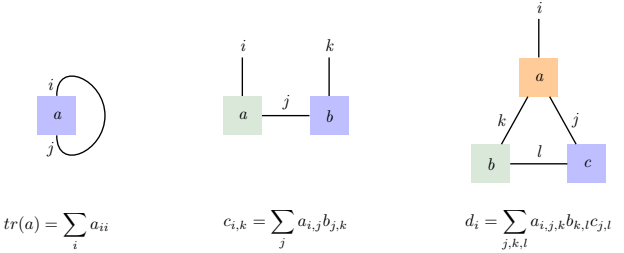


FIG. 28. Tensor diagram for tensor contraction.

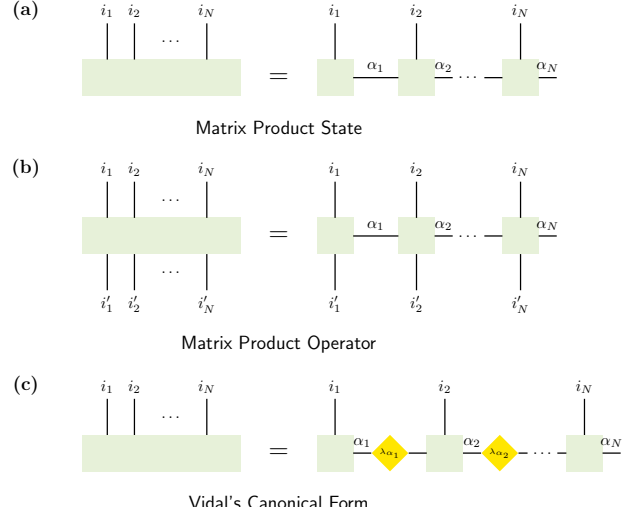


FIG. 29. Tensor diagram for MPS.

a state vector in a 2^N -dimensional space,

$$|\psi\rangle = \sum_{i_1, \dots, i_N} c_{i_1, \dots, i_N} |i_1 i_2 \dots i_N\rangle, \quad (29)$$

where each index $i_k \in \{0, 1\}$.

In quantum physics, the amplitude c_{i_1, \dots, i_N} is interpreted as a rank- N tensor with 2^N components. Since storing and manipulating this tensor directly becomes computationally intractable for even a modest number of qubits, we use the matrix product state (MPS) to provide an approximate representation of this tensor as a contracted network of smaller, lower-rank tensors, which in its open boundary condition (OBC) form reads [110]

$$c_{i_1, \dots, i_N} = \sum_{\alpha_1, \dots, \alpha_N=1}^{\chi} \Gamma_{\alpha_1}^{[1]i_1} \Gamma_{\alpha_1 \alpha_2}^{[2]i_2} \dots \Gamma_{\alpha_N}^{[N]i_N}. \quad (30)$$

Each $\Gamma^{[k]}$ represents a rank-3 tensor, and χ is the parameter called the bond dimension, which controls the accuracy of approximation. The virtual indices (α_{k-1}, α_k) are contracted and internal to the network, while the open physical index i_k corresponds to the local physical state at site k . For a qubit system, the physical dimension is

2. For a system in Fock space, the physical dimension is determined by the truncation of the local Hilbert space. The tensor diagram is shown in Fig. 29(a).

The MPS framework for states is naturally extended to operators via the Matrix Product Operator (MPO) representation, which is essential for encoding Hamiltonians and other observables. This is accomplished by augmenting each local tensor with a second physical index, transforming the MPS tensor $\Gamma_{\alpha_{k-1}\alpha_k}^{[k]i_k}$ into an MPO tensor $\Gamma_{\alpha_{k-1}\alpha_k}^{[k]i_k i'_k}$. The indices i_k and i'_k serve as the input and output physical indices, respectively, enabling the MPO to act as a linear map on the space of MPS. The tensor diagram is shown in Fig. 29(b).

The MPS representation of a quantum state is not unique due to a “gauge freedom”—an invertible matrix and its inverse can be inserted between any two adjacent tensors without altering the physical state. Vidal’s canonical form [111] eliminates this ambiguity by imposing specific orthogonality conditions, thereby providing a unique representation

$$c_{i_1, \dots, i_N} = \sum_{\alpha_1, \dots, \alpha_N=1}^{\chi} \Gamma_{\alpha_1}^{[1]i_1} \lambda_{\alpha_1}^{[1]} \Gamma_{\alpha_1 \alpha_2}^{[2]i_2} \lambda_{\alpha_2}^{[2]} \dots \Gamma_{\alpha_N}^{[N]i_N}. \quad (31)$$

To construct the MPS, we begin with the state’s coefficients, which form a rank- N tensor c_{i_1, \dots, i_N} . The first step involves reshaping this tensor into a matrix M_1 of dimensions $d \times d^{N-1}$, where d indicates the physical dimension. This is achieved by treating the first physical index i_1 as the row index, and grouping the remaining $N-1$ indices into a composite column index. Subsequently, a singular value decomposition (SVD) is applied to this matrix.

$$c_{i_1, i_2 i_3 \dots i_N} = \sum_{\alpha_1=1}^{\chi} \Gamma_{\alpha_1}^{[1]i_1} \lambda_{\alpha_1}^{[1]} V_{\alpha_1}^{[1]i_2 i_3 \dots i_N \dagger}. \quad (32)$$

This process is then iterated. For the second step, the unitary matrix $V^{[1]\dagger}$ obtained previously is reshaped into a new matrix M_2 with dimension $(d \cdot \chi) \times d^{N-2}$, where the indices (α_1, i_2) form the rows. SVD is applied to M_2 , yielding the next set of MPS tensors. This sequence of reshaping and applying SVD is repeated site by site until the entire state is decomposed into the MPS format.

The singular values, $\lambda_{\alpha_k}^{[k]}$, obtained at each step k are of profound physical significance. They are the Schmidt coefficients for the bipartition of the system into subsystems A (sites 1 to k) and B (sites $k+1$ to N). Consequently, they directly determine the bipartite entanglement entropy across this cut.

In large-scale simulations, we often set a global maximum bond dimension χ_{\max} and excessively small singular values are truncated after SVD. To exactly represent an arbitrary state, we require $\chi_{\max} > 2^{n/2}$ as emerging from SVD. However, far smaller bond dimensions precisely represent the ground state of 1-D systems that follow the area law of entanglement [112]. This reduces the

memory cost to store such a ground state from $\mathcal{O}(2^N)$ to $\mathcal{O}(N\chi^2)$.

DeepQuantum natively supports simulations using the MPS representation for both `QubitCircuit` and `QumodeCircuit`. To enable this functionality, simply set the `mps=True` flag during circuit initialization. The maximum bond dimension, which controls the simulation’s precision, is set as a global parameter using the `chi` argument.

For example, the following line of code creates a 20-qubit circuit with MPS bond dimension 7. The resulting quantum state is returned in its MPS form—a list of rank-3 tensors, where each tensor corresponds to a site in the quantum circuit.

```
1 cir = dq.QubitCircuit(nqubits=20, mps=True, chi
=7)
2 cir.cnot_ring()
3 mps_state = cir()
4 for state in mps_state:
5     print(state.shape)
```

```
torch.Size([1, 2, 2])
torch.Size([2, 2, 4])
torch.Size([4, 2, 7])
torch.Size([7, 2, 7])
.....
torch.Size([2, 2, 1])
```

Similarly, this functionality is also available for `QumodeCircuit`.

```
1 cir = dq.QumodeCircuit(nmode=20, init_state=[1] *
20, cutoff=4, backend='fock', basis=False,
mps=True, chi=3)
2 for i in range(nmode - 1):
3     cir.bs([i, i+1])
4 mps_state = cir()
5 for state in mps_state:
6     print(state.shape)
```

```
torch.Size([1, 4, 3])
torch.Size([3, 4, 3])
torch.Size([3, 4, 3])
.....
torch.Size([3, 4, 1])
```

B. Distributed Simulations

To address the exponential memory requirements of simulating large-scale quantum systems, DeepQuantum realizes a distributed parallel computing architecture [113] that leverages PyTorch’s native distributed communication package. This powerful feature allows the quantum state vector to be partitioned and managed across multiple processes or GPUs, supporting both intra-node and inter-node parallelism, thereby enabling the simulation of quantum systems at a scale that exceeds the memory limits of individual devices.

The framework is designed to facilitate a seamless transition from a single-device simulation to a distributed one. The primary change for the user is to replace the standard `QubitCircuit` class with its distributed counterpart, `DistributedQubitCircuit`. The API for constructing and executing the quantum circuit remains syntactically identical. This design philosophy allows developers to scale up their simulations with minimal code modification.

The example below illustrates the fundamental structure for a distributed simulation. The script is launched via `torchrun`, which manages the instantiation of processes. The `dq.setup_distributed()` function handles the initialization of the communication backend (e.g., ‘`nccl`’ for CUDA GPU), while `dq.cleanup_distributed()` ensures a clean shutdown.

Code 22. A minimal example of a distributed quantum circuit simulation. The script should be executed with the command `torchrun --nproc_per_node=[NUM_GPUS] script_name.py`.

```

1 import deepquantum as dq
2 import torch
3
4 # Initialize the distributed environment
5 rank, world_size, local_rank = dq.
6     setup_distributed(backend='nccl')
7 device = f'cuda:{local_rank}'
8 data = torch.arange(4, dtype=torch.float, device=
9     device, requires_grad=True)
10 # Construct the circuit
11 cir = dq.DistributedQubitCircuit(4)
12 cir.rylayer(encode=True)
13 cir.cnot_ring()
14 cir.observable(0)
15 cir.observable(1, 'x')
16 cir.to(device)
17 # Execute the simulation
18 state = cir(data).amps
19 result = cir.measure(with_prob=True)
20 exp = cir.expectation().sum()
21 exp.backward()
22 # Print the results gathered at rank 0
23 if rank == 0:
24     print(state)
25     print(result)
26     print(exp)
27     print(data.grad)
28 # Clean up the distributed process group
29 dq.cleanup_distributed()

```

As shown in Code 22, the core logic of simulating the quantum circuit is completely unchanged. `DistributedQubitCircuit` internally handles the complex task of partitioning the state vector and managing the inter-GPU communication required for gate operations that span across different state vector slices. `measure` and `expectation` automatically aggregate results from all processes and make them available on the rank-0 process, abstracting away the communication overhead from the user. The gradients of the expectation value with respect to parameters are calculated via the adjoint differentiation method by inheriting from `torch.autograd.Function`. This approach seamlessly integrates them into the whole computational

graph. Additionally, distributed simulations are also supported for the Fock backend based on state tensors via `DistributedQumodeCircuit`. Our framework combines the power of large-scale distributed computing with the simplicity and ease of use characteristic of DeepQuantum.

C. Applications

1. Simulation of Large Quantum System with MPS

The transverse-field Ising model (TFIM) with nearest-neighbor interactions is governed by the Hamiltonian [114]

$$\hat{H}_{\text{TFIM}} = \hat{H}_{ZZ} + \hat{H}_X = -J \sum_{\langle i,j \rangle} \hat{\sigma}_z^i \hat{\sigma}_z^j - h \sum_i \hat{\sigma}_x^i. \quad (33)$$

Choosing natural unit $\hbar = 1$, the time evolution of this Hamiltonian can be represented as a unitary operator

$$|\psi(t)\rangle = \hat{U}(t)\text{TFIM}|\psi(0)\rangle = \exp(-i\hat{H}_{\text{TFIM}}t)|\psi(0)\rangle. \quad (34)$$

To simulate this evolution on a digital quantum processor, it is necessary to perform Trotterization:

$$\begin{aligned} \exp(-i\hat{H}_{\text{TFIM}}t) &= \left(\exp(-i\hat{H}_{\text{TFIM}}\Delta t) \right)^N \\ &= \left(\exp\left(\frac{-i\hat{H}_X\Delta t}{2}\right) \exp(-i\hat{H}_{ZZ}\Delta t) \right. \\ &\quad \left. \exp\left(\frac{-i\hat{H}_X\Delta t}{2}\right) + \mathcal{O}(\Delta t^3) \right)^N, \end{aligned} \quad (35)$$

where $\Delta t = t/N$ and N is number of time steps. And the second equality is named second-order Trotterization [115, 116], with error scaling as $\mathcal{O}(\Delta t^3)$ [117].

The evolution of \hat{H}_{ZZ} and \hat{H}_X is implemented respectively with `QubitCircuit.rzz()` and `QubitCircuit.rx()` in DeepQuantum.

Evolution of the TFIM based on exact diagonalization is well-studied—the system can be mapped to free fermions using Jordan-Wigner and Bogoliubov transformations [114], which allows for studying the time dynamics of observables [118–120] under a quantum quench, *i.e.*, evolution under a Hamiltonian of which the initial state is not an eigenstate.

We study the quench of the TFIM using second-order Trotterization with the help of tensor networks. We use 45 qubits, a number beyond the boundary of classical exact diagonalization [1]. The state is initialized as $|+\rangle$ for all qubits, and we set the parameters as $J = 1.0$, $h = 1.2$, $\Delta t = 0.1$. The simulation is run under bond dimensions $\chi = 8, 16, 32, 64, 128$, and we track the evolution of the average X -magnetization $\overline{\langle \sigma_x^i \rangle}$ defined as

$$\overline{\langle \sigma_x^i \rangle} := \frac{1}{n} \sum_{i=1}^n \langle \hat{\sigma}_x^i \rangle, \quad (36)$$

where σ_x^i is Pauli- X operator on qubit i . Core implementation is demonstrated below.

Code 23. Matrix Product State for Time Evolution.

```

1  class TFIMSimulator:
2      def __init__(self, nqubit, J, h):
3          self.size = nqubit
4          self.J = J # coupling strength
5          self.h = h # transverse field
6
7      # Second-order Trotterization
8      def trotter_step(self, circuit, dt):
9          # X rotations (first half)
10         for i in range(self.size):
11             circuit.rx(i, self.h * dt)
12         # Even ZZ interactions
13         for i in range(0, self.size - 1, 2):
14             circuit.rzz([i, i+1], 2 * self.J * dt)
15
16         # Odd ZZ interactions
17         for i in range(1, self.size - 1, 2):
18             circuit.rzz([i, i+1], 2 * self.J * dt)
19
20         circuit.rzz([self.size - 1, 0], 2 * self.
21 J * dt)
22         # X rotations (second half)
23         for i in range(self.size):
24             circuit.rx(i, self.h * dt)
25         return circuit
26
27     # Evolve and measure TFIM
28     def quench(self, max_steps, dt, chi):
29         results = {}
30         steps, magnetizations = [], []
31
32         # Evolve step by step
33         for step in range(max_steps + 1):
34             cir = dq.QubitCircuit(self.size, mps=
35             True, chi=chi)
36             for i in range(self.size):
37                 cir.h(i)
38             for _ in range(step):
39                 cir = self.trotter_step(cir, dt)
40             for i in range(self.size):
41                 cir.observable(i, basis='x')
42
43             # Circuit execution
44             cir()
45             expectations = cir.expectation()
46             avg_mag = sum(exp.real for exp
47                 in expectations) / self.size
48             steps.append(step)
49             magnetizations.append(avg_mag)
50
51             results = {
52                 'steps': steps,
53                 'magnetization': magnetizations,
54                 'times': [s * dt for s in steps]
55             }
56         return results

```

The results are shown in Fig. 30. After the quench, the curve corresponding to the largest bond curve $\chi = 128$ indicates that the local observable $\langle \sigma_x^i \rangle$ relaxes in time, with expectation value approaching a stationary limit. This is due to dephasing between post-quench eigenstates, whose oscillations cancel out at long times [119, 120].

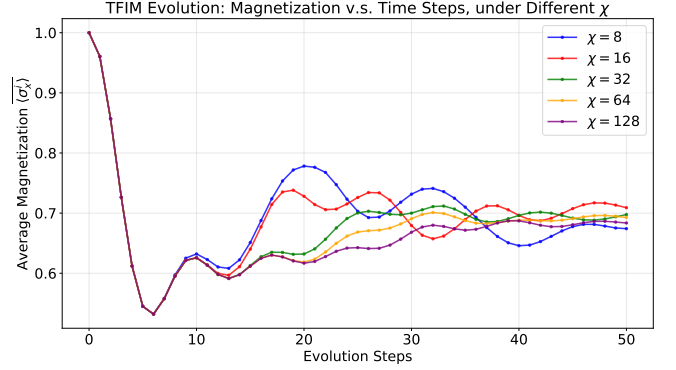


FIG. 30. Simulation of TFIM evolution under bond dimensions $\chi = 8, 16, 32, 64, 128$.

2. Distributed Quantum Fourier Transform

To further showcase the large-scale simulation capabilities of the framework, we implement a distributed quantum Fourier transform (QFT), a critical component in many quantum algorithms such as Shor's algorithm. The QFT circuit generates highly entangled states, making it a robust benchmark for the performance of a quantum simulator.

Code 24. Class-based implementation of a distributed QFT circuit.

```

1  import deepquantum as dq
2  import torch
3
4  class DistQFT(dq.DistributedQubitCircuit):
5      def __init__(self, nqubit):
6          super().__init__(nqubit=nqubit)
7          self.wires = list(range(nqubit))
8          for i in self.wires:
9              self.qft_block(i)
10
11     def qft_block(self, n):
12         self.h(n)
13         k = 2
14         for i in range(n, self.nqubit - 1):
15             self.cp(i + 1, n,
16                     torch.pi / 2 ** (k - 1))
17             k += 1

```

As shown in Code 24, the core of the circuit is the `qft_block` method, which recursively applies a Hadamard gate followed by a series of controlled phase rotations. This structure, which creates entanglement across all qubits, is expressed concisely using DeepQuantum's API.

We benchmark the performance of the distributed QFT simulation across 8 NVIDIA A100 GPUs for systems ranging up to 33 qubits. The execution time for a single forward pass of the circuit, followed by a measurement operation, is recorded. The results are based on the average of multiple runs to ensure consistency.

The results, summarized in Fig. 31, demonstrate the framework's ability to simulate these complex, highly en-

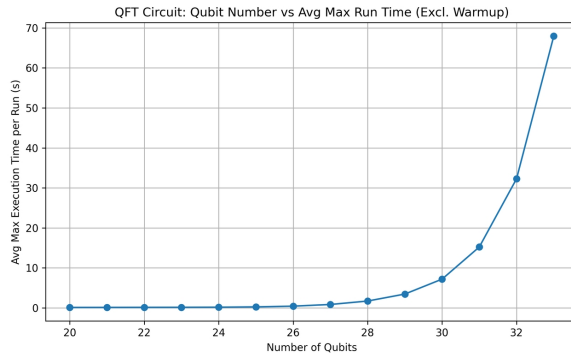


FIG. 31. Average execution time for the QFT simulation on 8 GPUs as a function of the number of qubits. The time is averaged over 10 runs for each data point (first run excluded). The exponential growth in simulation time reflects the complexity of the QFT circuit.

tangled states in a reasonable timeframe. Our benchmarks show that a 30-qubit QFT simulation completes in approximately 7.2 seconds, while a 33-qubit simulation—representing a state vector of 2^{33} complex amplitudes—is achieved in just over one minute.

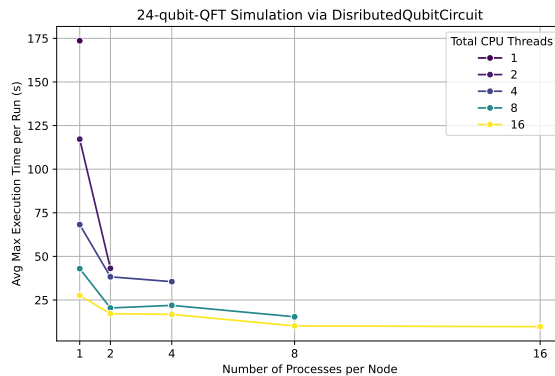


FIG. 32. Average execution time of the QFT simulation on a multi-core CPU for different configurations of parallelization and distribution hyperparameters.

Furthermore, the distributed computational workload is accelerated through a hybrid parallelization strategy—PyTorch’s distributed framework manages multi-process execution while leveraging OpenMP for intra-process parallelization of compute-intensive operations, thereby

efficiently utilizing all available CPU cores. To verify this, we perform simulations of a 24-qubit QFT on a multi-core CPU. The results in Fig. 32 indicate that an optimal configuration of parallelization and distribution hyperparameters yields a significant, multi-fold acceleration over serial execution.

These examples of performance underscore the effectiveness of DeepQuantum’s distributed architecture for tackling computationally demanding quantum simulations that are beyond the reach of conventional single-processor methods.

VIII. CONCLUSION

In this work, we have introduced DeepQuantum, a comprehensive software platform tailored for quantum machine learning and photonic quantum computing. By building directly upon PyTorch, DeepQuantum enables seamless integration of quantum components as native elements within dynamic computational graphs, allowing researchers to fully utilize PyTorch’s automatic differentiation, optimization tools, and rich machine learning ecosystem with minimal overhead. Uniquely, the platform provides a unified programming interface that integrates three fundamental paradigms of quantum computation: the conventional qubit-based model, DV and CV photonic quantum models, and the MBQC model. This integrated approach, supported by scalable tensor network simulations and distributed architecture, empowers users to explore a much broader landscape of hybrid algorithms and accelerate the discovery of AI-driven solutions for practical applications. Through various benchmarks and use cases, we have demonstrated DeepQuantum’s capability in variational algorithm implementation, photonic circuit simulation, and large-scale quantum computations, establishing it as a versatile and practical tool for advancing quantum information processing.

Looking forward, we plan to expand DeepQuantum’s library with more advanced photonic components, enhanced noise modeling capabilities, and improved hardware integration interfaces. Further optimization of computational performance and extended support for hybrid quantum-classical workflows are also key priorities. These developments will broaden the platform’s applicability, serving as a robust foundation for both academic research and industrial innovation in the evolving domains of AI-assisted QC and quantum-enhanced AI.

[1] Arute, F. *et al.* Quantum supremacy using a programmable superconducting processor. *Nature* **574**, 505–510 (2019).

[2] Wu, Y. *et al.* Strong quantum computational advantage using a superconducting quantum processor. *Physical review letters* **127**, 180501 (2021).

[3] Zhong, H.-S. *et al.* Quantum computational advantage using photons. *Science* **370**, 1460–1463 (2020).

[4] Preskill, J. Quantum computing in the nisq era and beyond. *Quantum* **2**, 79 (2018).

[5] Callison, A. & Chancellor, N. Hybrid quantum-classical algorithms in the noisy intermediate-scale quantum

era and beyond. *Phys. Rev. A* **106**, 010101 (2022). URL <https://link.aps.org/doi/10.1103/PhysRevA.106.010101>.

[6] Peruzzo, A. *et al.* A variational eigenvalue solver on a photonic quantum processor. *Nature communications* **5**, 4213 (2014).

[7] Farhi, E., Goldstone, J. & Gutmann, S. A quantum approximate optimization algorithm. *arXiv preprint arXiv:1411.4028* (2014).

[8] Ghosh, S., Opala, A., Matuszewski, M., Paterek, T. & Liew, T. C. Quantum reservoir processing. *npj Quantum Information* **5**, 35 (2019).

[9] Mujal, P. *et al.* Opportunities in quantum reservoir computing and extreme learning machines. *Advanced Quantum Technologies* **4**, 2100027 (2021).

[10] Dunjko, V., Taylor, J. M. & Briegel, H. J. Quantum-enhanced machine learning. *Physical review letters* **117**, 130501 (2016).

[11] Havlíček, V. *et al.* Supervised learning with quantum-enhanced feature spaces. *Nature* **567**, 209–212 (2019).

[12] Shor, P. W. Polynomial-time algorithms for prime factorization and discrete logarithms on a quantum computer. *SIAM review* **41**, 303–332 (1999).

[13] Grover, L. K. A fast quantum mechanical algorithm for database search. In *Proceedings of the twenty-eighth annual ACM symposium on Theory of computing*, 212–219 (1996).

[14] Andreasson, P., Johansson, J., Liljestrand, S. & Granath, M. Quantum error correction for the toric code using deep reinforcement learning. *Quantum* **3**, 183 (2019).

[15] Nautrup, H. P., Delfosse, N., Dunjko, V., Briegel, H. J. & Friis, N. Optimizing quantum error correction codes with reinforcement learning. *Quantum* **3**, 215 (2019).

[16] Fösel, T., Niu, M. Y., Marquardt, F. & Li, L. Quantum circuit optimization with deep reinforcement learning. *arXiv preprint arXiv:2103.07585* (2021).

[17] Pozzi, M. G., Herbert, S. J., Sengupta, A. & Mullins, R. D. Using reinforcement learning to perform qubit routing in quantum compilers. *ACM Transactions on Quantum Computing* **3**, 1–25 (2022).

[18] Acampora, G. *et al.* Quantum computing and artificial intelligence: status and perspectives. *arXiv preprint arXiv:2505.23860* (2025).

[19] Bergholm, V. *et al.* Pennylane: Automatic differentiation of hybrid quantum-classical computations. *arXiv preprint arXiv:1811.04968* (2018).

[20] Broughton, M. *et al.* Tensorflow quantum: A software framework for quantum machine learning. *arXiv preprint arXiv:2003.02989* (2020).

[21] Larsen, M. *et al.* Integrated photonic source of gottesman–kitaev–preskill qubits. *Nature* 1–5 (2025).

[22] Aghaee Rad, H. *et al.* Scaling and networking a modular photonic quantum computer. *Nature* **638**, 912–919 (2025).

[23] A manufacturable platform for photonic quantum computing. *Nature* **641**, 876–883 (2025).

[24] Raussendorf, R. & Briegel, H. J. A one-way quantum computer. *Physical review letters* **86**, 5188 (2001).

[25] Killoran, N. *et al.* Strawberry fields: A software platform for photonic quantum computing. *Quantum* **3**, 129 (2019).

[26] Kolarovszki, Z. *et al.* Piquasso: A photonic quantum computer simulation software platform. *Quantum* **9**, 1708 (2025).

[27] Heurtel, N. *et al.* Perceval: A software platform for discrete variable photonic quantum computing. *Quantum* **7**, 931 (2023).

[28] Sunami, S. & Fukushima, M. Graphix: optimizing and simulating measurement-based quantum computation on local-clifford decorated graph. *arXiv preprint arXiv:2212.11975* (2022).

[29] Paszke, A. *et al.* Pytorch: An imperative style, high-performance deep learning library. *Advances in neural information processing systems* **32** (2019).

[30] Hamilton, C. S. *et al.* Gaussian boson sampling. *Physical review letters* **119**, 170501 (2017).

[31] Xu, X. *et al.* Mindspore quantum: a user-friendly, high-performance, and ai-compatible quantum computing framework. *arXiv preprint arXiv:2406.17248* (2024).

[32] Gupt, B., Izaac, J. & Quesada, N. The walrus: a library for the calculation of hafnians, hermite polynomials and gaussian boson sampling. *Journal of Open Source Software* **4**, 1705 (2019).

[33] Zou, T. *et al.* Qpanda3: A high-performance software-hardware collaborative framework for large-scale quantum-classical computing integration. *arXiv preprint arXiv:2504.02455* (2025).

[34] Nocedal, J. & Wright, S. J. *Numerical optimization* (Springer, 2006).

[35] Cerezo, M. *et al.* Variational quantum algorithms. *Nature Reviews Physics* **3**, 625–644 (2021).

[36] Dirac, P. A. M. The quantum theory of the electron. *Proceedings of the Royal Society of London. Series A, Containing Papers of a Mathematical and Physical Character* **117**, 610–624 (1928).

[37] Quesada, N., Arrazola, J. M. & Killoran, N. Gaussian boson sampling using threshold detectors. *Physical Review A* **98**, 062322 (2018).

[38] Valiant, L. G. The complexity of computing the permanent. *Theoretical computer science* **8**, 189–201 (1979).

[39] Danos, V., Kashefi, E. & Panangaden, P. The measurement calculus. *Journal of the ACM (JACM)* **54**, 8–es (2007).

[40] Nielsen, M. A. & Chuang, I. L. *Quantum computation and quantum information* (Cambridge university press, 2010).

[41] Orús, R. A practical introduction to tensor networks: Matrix product states and projected entangled pair states. *Annals of physics* **349**, 117–158 (2014).

[42] He, K., Zhang, X., Ren, S. & Sun, J. Deep residual learning for image recognition. In *Proceedings of the IEEE conference on computer vision and pattern recognition*, 770–778 (2016).

[43] Wen, J., Huang, Z., Cai, D. & Qian, L. Enhancing the expressivity of quantum neural networks with residual connections. *Communications Physics* **7**, 220 (2024).

[44] Kashif, M. & Al-Kuwari, S. Resqnets: a residual approach for mitigating barren plateaus in quantum neural networks. *EPJ Quantum Technology* **11**, 1–28 (2024).

[45] Cong, I., Choi, S. & Lukin, M. D. Quantum convolutional neural networks. *Nature Physics* **15**, 1273–1278 (2019).

[46] Hur, T., Kim, L. & Park, D. K. Quantum convolutional neural network for classical data classification. *Quantum Machine Intelligence* **4**, 3 (2022).

[47] Minu, R., Margala, M., Shankar, S. S., Chakrabarti, P. & Nagarajan, G. Early-stage esophageal cancer detec-

tion using hybrid quantum cnn. *Soft Computing* 1–6 (2023).

[48] Chen, G. *et al.* Quantum convolutional neural network for image classification. *Pattern Analysis and Applications* **26**, 655–667 (2023).

[49] Kok, P. *et al.* Linear optical quantum computing with photonic qubits. *Reviews of modern physics* **79**, 135–174 (2007).

[50] O'brien, J. L. Optical quantum computing. *Science* **318**, 1567–1570 (2007).

[51] Gisin, N. & Thew, R. Quantum communication. *Nature photonics* **1**, 165–171 (2007).

[52] Braunstein, S. L. & Van Loock, P. Quantum information with continuous variables. *Reviews of modern physics* **77**, 513–577 (2005).

[53] Bartlett, S. D., Sanders, B. C., Braunstein, S. L. & Nemoto, K. Efficient classical simulation of continuous variable quantum information processes. *Physical Review Letters* **88**, 097904 (2002).

[54] Weedbrook, C. *et al.* Gaussian quantum information. *Reviews of Modern Physics* **84**, 621–669 (2012).

[55] Ferraro, A., Olivares, S. & Paris, M. G. Gaussian states in continuous variable quantum information. *arXiv preprint quant-ph/0503237* (2005).

[56] Lloyd, S. & Braunstein, S. L. Quantum computation over continuous variables. *Physical Review Letters* **82**, 1784 (1999).

[57] Bartlett, S. D. & Sanders, B. C. Universal continuous-variable quantum computation: Requirement of optical nonlinearity for photon counting. *Physical Review A* **65**, 042304 (2002).

[58] Ourjoumtsev, A., Jeong, H., Tualle-Brouri, R. & Grangier, P. Generation of optical ‘schrödinger cats’ from photon number states. *Nature* **448**, 784–786 (2007).

[59] Lvovsky, A. I. & Raymer, M. G. Continuous-variable optical quantum-state tomography. *Reviews of modern physics* **81**, 299–332 (2009).

[60] Gottesman, D., Kitaev, A. & Preskill, J. Encoding a qubit in an oscillator. *Physical Review A* **64**, 012310 (2001).

[61] Yokoyama, S. *et al.* Ultra-large-scale continuous-variable cluster states multiplexed in the time domain. *Nature Photonics* **7**, 982–986 (2013).

[62] Alexander, R. N. & Menicucci, N. C. Flexible quantum circuits using scalable continuous-variable cluster states. *Physical Review A* **93**, 062326 (2016).

[63] Asavanant, W. *et al.* Generation of time-domain-multiplexed two-dimensional cluster state. *Science* **366**, 373–376 (2019).

[64] Barenco, A. *et al.* Elementary gates for quantum computation. *Physical review A* **52**, 3457 (1995).

[65] Pittman, T., Jacobs, B. & Franson, J. Probabilistic quantum logic operations using polarizing beam splitters. *Physical Review A* **64**, 062311 (2001).

[66] Ralph, T. C., Langford, N. K., Bell, T. & White, A. Linear optical controlled-not gate in the coincidence basis. *Physical Review A* **65**, 062324 (2002).

[67] O'Brien, J. L., Pryde, G. J., White, A. G., Ralph, T. C. & Branning, D. Demonstration of an all-optical quantum controlled-not gate. *Nature* **426**, 264–267 (2003).

[68] Russell, N. J., Chakhmakhchyan, L., O'Brien, J. L. & Laing, A. Direct dialling of haar random unitary matrices. *New journal of physics* **19**, 033007 (2017).

[69] Reck, M., Zeilinger, A., Bernstein, H. J. & Bertani, P. Experimental realization of any discrete unitary operator. *Physical review letters* **73**, 58 (1994).

[70] Carolan, J. *et al.* Universal linear optics. *Science* **349**, 711–716 (2015).

[71] Bogaerts, W. *et al.* Programmable photonic circuits. *Nature* **586**, 207–216 (2020).

[72] Clements, W. R., Humphreys, P. C., Metcalf, B. J., Kolthammer, W. S. & Walmsley, I. A. Optimal design for universal multiport interferometers. *Optica* **3**, 1460–1465 (2016).

[73] Brod, D. J. *et al.* Photonic implementation of boson sampling: a review. *Advanced Photonics* **1**, 034001–034001 (2019).

[74] Bulmer, J. F. *et al.* The boundary for quantum advantage in gaussian boson sampling. *Science advances* **8**, eab19236 (2022).

[75] Zhong, H.-S. *et al.* Phase-programmable gaussian boson sampling using stimulated squeezed light. *Physical review letters* **127**, 180502 (2021).

[76] Madsen, L. S. *et al.* Quantum computational advantage with a programmable photonic processor. *Nature* **606**, 75–81 (2022).

[77] Banchi, L., Fingerhuth, M., Babej, T., Ing, C. & Arrazola, J. M. Molecular docking with gaussian boson sampling. *Science advances* **6**, eaax1950 (2020).

[78] Schuld, M., Brádler, K., Israel, R., Su, D. & Gupt, B. Measuring the similarity of graphs with a gaussian boson sampler. *Physical Review A* **101**, 032314 (2020).

[79] Arrazola, J. M. & Bromley, T. R. Using gaussian boson sampling to find dense subgraphs. *Physical review letters* **121**, 030503 (2018).

[80] Oh, C., Fefferman, B., Jiang, L. & Quesada, N. Quantum-inspired classical algorithm for graph problems by gaussian boson sampling. *PRX quantum* **5**, 020341 (2024).

[81] Brádler, K., Dallaire-Demers, P.-L., Rebentrost, P., Su, D. & Weedbrook, C. Gaussian boson sampling for perfect matchings of arbitrary graphs. *Physical Review A* **98**, 032310 (2018).

[82] Einstein, A., Podolsky, B. & Rosen, N. Can quantum-mechanical description of physical reality be considered complete? *Physical review* **47**, 777 (1935).

[83] Greenberger, D. M. Ghz (greenberger–horne–zeilinger) theorem and ghz states. In *Compendium of quantum physics*, 258–263 (Springer, 2009).

[84] Reid, M. D. *et al.* Colloquium: the einstein-podolsky-rosen paradox: from concepts to applications. *Reviews of Modern Physics* **81**, 1727–1751 (2009).

[85] Takeda, S., Takase, K. & Furusawa, A. On-demand photonic entanglement synthesizer. *Science advances* **5**, eaaw4530 (2019).

[86] Yoshikawa, J.-i. *et al.* Invited article: Generation of one-million-mode continuous-variable cluster state by unlimited time-domain multiplexing. *APL photronics* **1** (2016).

[87] Aoki, T. *et al.* Quantum error correction beyond qubits. *Nature Physics* **5**, 541–546 (2009).

[88] Menicucci, N. C. Fault-tolerant measurement-based quantum computing with continuous-variable cluster states. *Physical review letters* **112**, 120504 (2014).

[89] Weigand, D. J. & Terhal, B. M. Realizing modular quadrature measurements via a tunable photon-pressure coupling in circuit qed. *Physical Review A* **101**,

053840 (2020).

[90] Raussendorf, R. & Briegel, H. J. A one-way quantum computer. *Physical review letters* **86**, 5188 (2001).

[91] Raussendorf, R., Browne, D. E. & Briegel, H. J. Measurement-based quantum computation on cluster states. *Physical review A* **68**, 022312 (2003).

[92] Walther, P. *et al.* Experimental one-way quantum computing. *Nature* **434**, 169–176 (2005).

[93] Browne, D. E. & Rudolph, T. Resource-efficient linear optical quantum computation. *Physical Review Letters* **95**, 010501 (2005).

[94] Van den Nest, M., Miyake, A., Dür, W. & Briegel, H. J. Universal resources for measurement-based quantum computation. *Physical review letters* **97**, 150504 (2006).

[95] Raussendorf, R., Harrington, J. & Goyal, K. A fault-tolerant one-way quantum computer. *Annals of physics* **321**, 2242–2270 (2006).

[96] Varnava, M., Browne, D. E. & Rudolph, T. Loss tolerance in one-way quantum computation via counterfactual error correction. *Physical review letters* **97**, 120501 (2006).

[97] Menicucci, N. C. Fault-tolerant measurement-based quantum computing with continuous-variable cluster states. *Physical review letters* **112**, 120504 (2014).

[98] Broadbent, A., Fitzsimons, J. & Kashefi, E. Universal blind quantum computation. In *2009 50th annual IEEE symposium on foundations of computer science*, 517–526 (IEEE, 2009).

[99] Barz, S. *et al.* Demonstration of blind quantum computing. *science* **335**, 303–308 (2012).

[100] Vidal, G. Efficient classical simulation of slightly entangled quantum computations. *Physical review letters* **91**, 147902 (2003).

[101] Vidal, G. Classical simulation of infinite-size quantum lattice systems in one spatial dimension. *Physical review letters* **98**, 070201 (2007).

[102] Orus, R. & Vidal, G. Infinite time-evolving block decimation algorithm beyond unitary evolution. *Physical Review B—Condensed Matter and Materials Physics* **78**, 155117 (2008).

[103] Shi, Y.-Y., Duan, L.-M. & Vidal, G. Classical simulation of quantum many-body systems with a tree tensor network. *Physical Review A—Atomic, Molecular, and Optical Physics* **74**, 022320 (2006).

[104] Haegeman, J., Lubich, C., Oseledets, I., Vandereycken, B. & Verstraete, F. Unifying time evolution and optimization with matrix product states. *Physical Review B* **94**, 165116 (2016).

[105] Markov, I. L. & Shi, Y. Simulating quantum computation by contracting tensor networks. *SIAM Journal on Computing* **38**, 963–981 (2008).

[106] Evenbly, G. & Vidal, G. Algorithms for entanglement renormalization. *Physical Review B—Condensed Matter and Materials Physics* **79**, 144108 (2009).

[107] Brandão, F. G. & Horodecki, M. An area law for entanglement from exponential decay of correlations. *Nature physics* **9**, 721–726 (2013).

[108] Eisert, J., Cramer, M. & Plenio, M. B. Colloquium: Area laws for the entanglement entropy. *Reviews of modern physics* **82**, 277–306 (2010).

[109] Penrose, R. *et al.* Applications of negative dimensional tensors. *Combinatorial mathematics and its applications* **1**, 3 (1971).

[110] Cirac, J. I., Perez-Garcia, D., Schuch, N. & Verstraete, F. Matrix product states and projected entangled pair states: Concepts, symmetries, theorems. *Reviews of Modern Physics* **93**, 045003 (2021).

[111] Vidal, G. Efficient classical simulation of slightly entangled quantum computations. *Physical review letters* **91**, 147902 (2003).

[112] Verstraete, F. & Cirac, J. I. Matrix product states represent ground states faithfully. *Physical Review B—Condensed Matter and Materials Physics* **73**, 094423 (2006).

[113] Jones, T., Koczor, B. & Benjamin, S. C. Distributed simulation of statevectors and density matrices. *arXiv preprint arXiv:2311.01512* (2023).

[114] Pfeuty, P. The one-dimensional ising model with a transverse field. *ANNALS of Physics* **57**, 79–90 (1970).

[115] Suzuki, M. General theory of higher-order decomposition of exponential operators and symplectic integrators. *Physics Letters A* **165**, 387–395 (1992).

[116] Berry, D. W., Ahokas, G., Cleve, R. & Sanders, B. C. Efficient quantum algorithms for simulating sparse hamiltonians. *Communications in Mathematical Physics* **270**, 359–371 (2007).

[117] Childs, A. M., Su, Y., Tran, M. C., Wiebe, N. & Zhu, S. Theory of trotter error with commutator scaling. *Physical Review X* **11**, 011020 (2021).

[118] Barouch, E., McCoy, B. M. & Dresden, M. Statistical mechanics of the xy model. i. *Physical Review A* **2**, 1075 (1970).

[119] Barouch, E. & McCoy, B. M. Statistical mechanics of the x y model. ii. spin-correlation functions. *Physical Review A* **3**, 786 (1971).

[120] Barouch, E. & McCoy, B. M. Statistical mechanics of the xy model. iii. *Physical Review A* **3**, 2137 (1971).

ACKNOWLEDGMENTS

This research is supported by the National Key R&D Program of China (Grants No. 2024YFB4504005, No. 2024YFA1409300); National Natural Science Foundation of China (NSFC) (Grants No. 62235012, No. 12304342, No. 12574549, No. 12574542, No. 125B1033); Innovation Program for Quantum Science and Technology (Grants No. 2021ZD0301500, and No. 2021ZD0300700); Science and Technology Commission of Shanghai Municipality (STCSM) (Grants No. 2019SHZDZX01, No. 24ZR1438700, No. 24ZR1430700 and No. 24LZ1401500); Startup Fund for Young Faculty at SJTU (SFYF at SJTU) (Grants No. 24X010502876 and No. 24X010500170); Frontier Technologies R&D Program of Jiangsu (Grant No. SBF20250000094); Zhiyuan Future Scholar Program (Grant No. ZIRC2024-06). X.-M.J. acknowledges additional support from a Shanghai talent program and support from Zhiyuan Innovative Research Center of Shanghai Jiao Tong University. H. T. acknowledges additional support from Yangyang Development Fund.